

# **Interactive comment on “The optical, physical properties and direct radiative forcing of urban columnar aerosols in Yangtze River Delta, China”**

**by Bingliang Zhuang et al.**

**Anonymous Referee #3**

Received and published: 30 July 2017

Aerosols have significant impacts on air quality and global climate change and their influences have considerably uncertainties due to the spatial-temporal variations of the aerosol optical properties. This manuscript presents the observed results of the aerosol optical and physical properties in an urban site in the YRD region, and estimates the aerosol direct radiative accordingly. The methods are reliable and the results are helpful to improve the model performance on the aerosol climate effects. I think the manuscript can be accepted after the following concerns are addressed.

**To anonymous Referee #3:**

Dear reviewer, thank you very much for reviewing the manuscript and providing us the important comments and suggestions on our study. With respect to your comments, substantial improvements and revisions of the paper have been made. We will response to your comments carefully point by point; details of the revisions can be referred to the new version of the manuscript.

**Relevant changes of the revised manuscript (marked with traces) are enclosed in the last part of this document.**

**Major comments:**

1. Plenty of data and results are presented in the manuscript. Just as summarized by the authors, altogether nine types of aerosols' optical properties are discussed. In addition, DRF of aerosols are also presented and discussed. The authors are encouraged to clarify the most important finding(s) of this study. Also, the novelty of the study should be strengthened.

**R:** According to your comments and suggestions, the manuscript has been rephrased throughout the whole text. In revised version, the key finding(s) and novelty of this study have been reflected in a better way in several parts of the manuscript, including in the sections of Abstract, Introduction, Discussions, as well as Conclusion. Details can be found in the revised manuscript.

2. I think the manuscript (including the figures and tables) is too long to catch the key information. It is suggested that many parts of the manuscript (such as Section 3.1.1, the conclusion and so on) should be shortened and some parts (such as Section 3.1.2, Table 1 and so on) should be moved to the supplemental materials at least if not deleted.

**R:** Thank you for your suggestions. Most parts of the manuscript have been shortened, especially for the Sections 3.1.1, 3.1.2, 3.4.1 and 4, to make it more clearly and readable. Figures 4, 5, 6 in original version have been also simplified and merged into a new figure (Figure 4) in revised version. More details can be found in the revised manuscript. The authors suggest that the values are necessary to be listed in the tables, which is more conveniently and easily for the readers to use the data of the

observations.

3. A more in-depth discussion on aerosol classification (Section 3.3) should be provided, such as their uncertainties, since optical properties of aerosols are highly dependent on the chemical compositions and mixing state and so on.

**R:** According to your suggestion, Section 3.3 has been extended to degrees. More in-depth discussions on the aerosol classification and identification have been included in the current version. More details can be found in the revised manuscript.

4. What are the vertical resolutions of aerosol profiles from CALIPSO and Lidar? And what is the spatial resolution of CALIPSO? Why did the authors choose CALIPSO to represent the aerosol profile at the urban site?

**R:** For CALIPSO, its resolution is 30 m vertically and 333 m horizontally. For Lidar, its vertical resolution is 3.75-7.5 m.

With respect to your third question here, we do not choose CALIPSO to represent the aerosol profile purely. Instead, both the profiles of CALIPSO and Lidar are all used in this study to access the aerosol direct radiative forcing (DRF) as presented at the beginning of Section 3.4. Compared with CALIPSO, the Lidar observation in Nanjing has only been conducted in several times in some seasons. Thus, the Lidar observed aerosol profile could not fully represent the whole conditions of vertical aerosols in Nanjing. And the CALIPSO could make up such deficiency to degrees. Additionally, the aerosol profiles from different observed platforms show substantial differences. Therefore, both the profiles of CALIPSO and Lidar are adopted here. And sensitivities of the aerosol DRF to the profiles are further carried out to quantify the influence of the profiles on DRFs.

5. I have to repeat that the conclusion is too long and many sentences in this part are redundant. It should be shortened.

**R:** Thanks again, this section has been shortened significantly and it's more clearly to reflect the analysis on the results and more readable to the readers. More details can be found in the revised manuscript.

6. What are the inter-annual variations of the aerosol optical properties and direct radiative forcing in urban area of Nanjing?

**R:** Thank you for your question. A much longer observation is needed to ensure a sufficient sample size (such as in Che et al., 2015) if the inter-annual or –decadal variations of the aerosol optical properties and DRF would be further investigated. Therefore, investigation on the inter-annual variations of the aerosol optical properties and DRFs do not belong to the scope of current study.

#### **Reference:**

Che, H. Z., Zhang, X. Y., Xia, X., Goloub, P., Holben, B., Zhao, H., Wang, Y., Zhang, X. C., Wang, H., Blarel, L., Damiri, B., Zhang, R., Deng, X., Ma, Y., Wang, T., Geng, F., Qi, B., Zhu, J., Yu, J., Chen, Q., and Shi, G.: Ground-based aerosol climatology of China: aerosol optical depths from the China Aerosol Remote Sensing Network (CARSNET) 2002–2013, *Atmos. Chem. Phys.*, 15, 7619–7652, 2015

7. There are still some grammatical errors. The editing and proofreading of the manuscript by a native English speaker is highly recommended.

**R:** Thanks for your advice. The manuscript has been rephrased throughout the whole text to make it more clearly as mentioned above. And it's also corrected carefully by Professor J. Liu, who is from University of Toronto and also is a co-author of this study with great contributions.

**Specific comments:**

1. The title is confusing. What is "urban columnar aerosols"? Does it refer to aerosols emitted from urban area or aerosols in urban area? It is suggested to reword the title.

**R:** Thanks for your question. It means the aerosols in urban area.

2. The period of study seems to be not clearly mentioned in the manuscript.

**R:** The period of the study is described in second paragraph of Section 2.1.

3. Why Fig. 7 shows larger error bar for CE-318 derived AOD than MODIS derived AOD?

**R:** The larger error bars for CE-318 in (original) Figure 7 is possibly resulted from a higher temporal resolution of the ground based observation compared with the satellites.

4. Why the profiles are shown in terms of percentage instead of extinction coefficient?

**R:** To make a comparison among different observations or values, all profiles in the figure are standardized to the percentage (%).

5. Line 59-62: Rewrite this sentence to make it clear.

**R:** The sentence has been rewritten.

6. Line 64-105: Make this paragraph more concise and do NOT list the results of each study.

**R:** This paragraph has been rephrased in the revised manuscript.

7. Line 112-121: Move this part to the Section 2 (Methodologies).

**R:** These sentences have been deleted in Introduction of the revised manuscript.

8. Which kind of aerosols did the Aethalometer measure? Fine particles or total aerosols? Please clarify.

**R:** It's for total aerosols. And it has been clarified in Section 2.

1 **The optical, physical properties and direct radiative forcing of**  
2 **urban columnar aerosols in Yangtze River Delta, China**

3 Bingliang Zhuang<sup>1,\*</sup>, Tijian Wang<sup>1,\*\*</sup>, Jane. Liu<sup>1,2</sup>, Huizheng Che<sup>3</sup>, Yong Han<sup>1</sup>, Yu Fu<sup>4</sup>,  
4 Shu Li<sup>1</sup>, Min Xie<sup>1</sup>, Mengmeng Li<sup>1</sup>, Pulong Chen<sup>1</sup>, Huimin Chen<sup>1</sup>, Xiu-qun Yang<sup>1</sup>,  
5 Jianning Sun<sup>1</sup>

6 <sup>1</sup> School of Atmospheric Sciences, CMA-NJU Joint Laboratory for Climate Prediction Studies, Jiangsu  
7 Collaborative Innovation Center for Climate Change, Nanjing University, Nanjing 210023, China

8 <sup>2</sup> Department of Geography and Planning, University of Toronto, Toronto, M5S 3G3, Canada

9 <sup>3</sup> Key Laboratory of Atmospheric Chemistry (LAC), Chinese Academy of Meteorological Sciences (CAMS),  
10 CMA, Beijing, 100081, China

11 <sup>4</sup> Dalian Weather Modification Office, Dalian, 116001, China

12 \* Corresponding author, E-mail: [blzhuang@nju.edu.cn](mailto:blzhuang@nju.edu.cn); Tel.: +862589681156; fax: +862589683797

13 \*\* Corresponding author, E-mail: [tjwang@nju.edu.cn](mailto:tjwang@nju.edu.cn); Tel.: +862589683797; fax: +862589683797

14

15 **Abstract:** The fractionated aerosol optical and physical properties as well as its direct radiative forcing  
16 (DRF) in urban area of west Yangtze River Delta (YRD)Nanjing (urNJ) are investigated, based on the  
17 measurements of Cimel sun-photometer combined with a radiation transfer model. Ground based  
18 observed aerosols have much higher temporal resolutions compared with satellite retrievals. Analysis  
19 firstly reveals the characteristics of fractionated aerosol optical properties of different aerosol types in  
20 west YRD. We find that tThe annual mean 550-nm-aerosol optical depth (AOD) of the total aerosols is  
21 about  $0.65 \pm 0.28$ , dominated by the scattering aerosols (about  $94\%$   $93.8\%$ ), with a mean refractive index  
22 of  $1.44 + 0.0084i$  at 440 nm, resulting in a mean single scattering albedo (SSA) of 0.93 at 550 nm and  
23 refractive index of  $1.44 + 0.0084i$  at 440 nm during the sampling period. The fine aerosols are about 4  
24 times to, and also have very different compositions from the coarse ones. The absorbing components

25 only account for ~4.6% in fine aerosols while 15.5% in coarse aerosols, but within the same mode, they  
26 have smaller sizes than scattering aerosols. The scattering aerosol has larger size than the absorbing  
27 aerosol, with Ångström exponents (AE) of 1.19 at 440/870 nm, 0.13 smaller than the latter one. The  
28 coarse mode fraction for the scattering aerosol (18.03%) is much smaller than the absorbing aerosol's  
29 (43.91%). Therefore, the fine mode aerosol particles are much ~~present~~ presents more scattering (SSA=0.95)  
30 while than the coarse ~~one~~ aerosol is more absorption (SSA=0.82), simultaneously reflecting that each  
31 component has different size distributions. Relationships among the optical properties quantify the  
32 aerosol mixings and they imply. Analysis implies that there are about 15% and 27.5% occurrences of  
33 dust and black carbon dominated mixing aerosols, respectively, ~~during the sampling period in west~~  
34 YRD. Different from optical properties, aerosols in west YRD have the similar volume size  
35 distributions to the ones in other sites over east China climatologically. All the optical properties follow  
36 a simple unimodal pattern. Aerosols in urNJ have a two-mode lognormal pattern in volume size  
37 distribution, peaking at the radius of 0.148 and 2.94  $\mu\text{m}$ , and the AOD positively depends on them. But  
38 analysis further reveals that the fine or coarse dominated particles could individually lead to severe  
39 haze pollutions in YRD. Although the fine mode aerosol has a much smaller sizes than the coarse one,  
40 they have the same level of the volume concentrations (about  $0.12 \mu\text{m}^3/\text{cm}^3$ ) due to much higher  
41 fraction of the fine aerosol. Observed based estimations indicate that both the fine and coarse aerosols  
42 in west YRD exert a negative DRF, especially for the former one ( $-11.17 \text{ W/m}^2$  at the top of atmosphere,  
43 TOA). A higher absorption fraction directly leads to the negative DRF being offset more substantially  
44 for coarse aerosols ( $-0.33 \text{ W/m}^2$ ) at the TOA. Similarly, the coarse mode DRF only contributes to ~14%  
45 within scattering aerosols while >34% within absorbing aerosols. Estimations present that the mean  
46 aerosol DRFs at the top of atmosphere (TOA) are  $-10.69, -16.45, +5.76 \text{ W/m}^2$ , respectively, for the total,

47 scattering and absorbing aerosols in clear sky. At the surface, the DRFs are 1.1–2.5 times stronger than  
48 those at TOA, and the fine aerosol DRFs in these three type of aerosols account for 83.7%, 91.7% and  
49 67.2%, respectively, to their totals. Sensitive analysis states that Normally, aerosol DRFs is not very  
50 sensitive (no more than 5%) to its profiles in clear sky condition (extreme cases excepted), although  
51 both aerosol scattering and absorption could become weaker to some extent if more aerosols were in  
52 lower layers. Both the aerosol properties and DRFs have substantial seasonality in west YRD. Results  
53 further reveal the contributions of each component in different size segments to the total AODs and  
54 DRFs. Also they are advantageous to improve the model performances on the aerosol and its effects in  
55 east regions of China.

## 57 1 Introduction

58 Atmospheric aerosols have significant influences on air quality, human health, and regional/global  
59 climate changes. Their loadings in the global atmosphere have increased substantially in recent years.  
60 Scientists suggested that the scattering aerosols, such as sulfate and nitrate, could greatly offset the  
61 warming effects of greenhouse gases (Kiehl and Briegleb, 1993) while the absorbing  
62 aerosol components, such as black carbon (BC), might further exacerbate the global warming  
63 (Jacobson 2002). The global mean direct radiative forcings (DRF) of scattering aerosols, fossil fuel BC  
64 and the total aerosols were was estimated to be about -0.55, +0.2, -1.04 W/m<sup>2</sup>, respectively (Forster et  
65 al., 2007; Reddy et al., 2005) at the top of atmosphere (TOA), thus changing the atmospheric  
66 circulations and hydrological cycle would be further affected when the radiation balance is changed by  
67 the aerosols. Menon et al. (2002) suggested that changes in the trend of rainfall in China over the past 5  
68 decades might be related to the variation of BC in southern and eastern Asia regions. Wang et al. (2015)

69 indicates that the East Asia summer monsoon circulation could become weaker due to the cooling  
70 effects of the aerosols but stronger due to the warming effects of BC.

71 Although many studies on the aerosol radiative forcing and climate effects have been carried out  
72 in both global and regional scales based on model simulations and observations in the past two decades  
73 (e.g., Penner et al., 2001; Bellouin et al., 2003; Liao and Seinfeld, 2005; Wu et al., 2012; Wang et al.,  
74 2015; etc.), large uncertainties still exist. Forster et al. (2007) pointed out that the global mean ~~direct~~  
75 ~~radiative forcing~~DRF varied from +0.04 to -0.63 W/m<sup>2</sup> for the total aerosols and from +0.1 to +0.3  
76 W/m<sup>2</sup> for BC. The ranges were larger in regional scales, especially in high aerosol emitted regions  
77 (Zhuang et al., 2013a). ~~Zhuang et al. (2013a) indicated that the simulated BC direct radiative forcing~~  
78 ~~varied from +0.32 to +0.81 W/m<sup>2</sup> over East Asia.~~ The DRF uncertainties would subsequently result in  
79 large bias ~~when assessing of~~ the aerosol climate effects. ~~There are many key~~ factors affecting the  
80 simulated radiative forcing, including ~~are~~ the aerosol optical properties, which are related to the aerosol  
81 emissions, size distributions, profiles, compositions, and mixing states (Holler et al., 2003; Ma et al.,  
82 2017), surface albedo and clouds (Ma and Yu, 2012; Forster et al., 2007). The uncertainties could be  
83 reduced substantially if the observed aerosol optical properties were figured out and were used ~~when~~  
84 ~~calculating the forcing~~ (Forster et al., 2007).

85 With the rapid increase in population and growth in economics, the air pollutant~~trace gases and~~  
86 ~~particulate matter~~ emissions are much higher in East Asia than in the other regions (Zhang et al., 2009).  
87 Additionally, dust aerosols from desert regions~~northwest China and Mongolia~~ are always transported to  
88 north and east China or even further afield (Wang et al., 2009; Sun et al., 2012; Li et al., 2015a).  
89 Consequently, aerosols in China become frequently large in loadings and complicated in compositions  
90 and spatial distributions (Zhang et al., 2012), especially in urban agglomerations or megacities (e.g.:

91 Yangtze River Delta: YRD). Therefore, it is necessary to clarify study the aerosol optical properties ~~and~~  
92 radiative forcing in YRD through observations, which is a premise for accurately estimating the aerosol  
93 radiative -climate effects and also in favor of improving the model performance on aerosols -in East  
94 east region of ChinaAsia. Recently, substantial observation-based studies have conducted on both the  
95 surface (e.g., Bergin et al., 2001; Xu et al., 2002; Zhang et al., 2004; Xia et al., 2007; Yan et al., 2008;  
96 He et al., 2009; Fan et al., 2010; Cai et al., 2011; Xu et al., 2012; Wu et al., 2012; Zhang et al., 2015;  
97 Yu et al., 2016; Deng et al., 2016; etc.) and columnar (e.g., Chiang et al., 2007; Pan et al., 2010; Yu et  
98 al., 2011; Zhao et al., 2013; Tao et al., 2014; Zhu et al., 2014; Che et al., 2011; 2013; 2014; 2015a, b, c;  
99 Xia et al., 2016; Zheng et al., 2016; Qi et al., 2016, etc.) aerosol optical properties (and ~~direct radiative~~  
100 ~~forcing~~DRFs), especially ~~on aerosols~~ in China. However, surface data could not completely represent  
101 the whole conditions of the aerosols in atmosphere and they are highly affected by the variations of  
102 boundary layers. Its deficiency could be made up by the measurements of the columnar aerosols. For  
103 the studies of surface aerosols, people mainly focus on their absorption and scattering coefficients  
104 (AAC and SC). Investigations state that the annual mean aerosol absorption coefficient (AAC) at 532  
105 nm was about 56 Mm<sup>-1</sup> in urban area of Beijing from 2005 to 2006 (He et al. 2009) and it was about  
106 41-44 Mm<sup>-1</sup> at an urban site of YRD from 2012 to 2013 (Zhuang et al., 2015). The annual mean  
107 aerosol scattering coefficients (SC) at 520 nm and AAC at 532 nm were 525 and 83 Mm<sup>-1</sup>, respectively,  
108 in Xi'an in 2009 and were 456 and 96 Mm<sup>-1</sup>, respectively, in Chengdu in 2011. Both AACs and SCs in  
109 urban areas are frequently stronger than those at other sites. They AAC and SC were 17.5~30 and  
110 174.6338 Mm<sup>-1</sup> in rural area of Beijingwest YRD (Yan et al., 2008Zhuang et al., 2017) and they were 6  
111 and 158 Mm<sup>-1</sup>, respectively in desert region (Xu et al., 2004). For columnar aerosol observations, the  
112 detailed aerosol optical and physical properties could be obtained, including optical depth (AOD).



113 refractive index, Ångström exponents (AE), and so on. Che et al. (2015a) introduced a systematic  
114 long-term measurement of the countrywide total aerosol AOD and AE in China from 2002 to 2013, and  
115 indicated that annual mean AOD were 0.14, 0.74 and 0.54 at the rural sites, urban sites, and in east  
116 China, respectively. In YRD, Pan et al. (2010) shows that optical depths (AOD) at 440 nm and  
117 Ångström exponents (AE) in coastal area (east YRD) of the Yangtze River Delta (YRD) was about 0.74  
118 and 1.27, respectively. Yu et al. (2011) and Qi et al. (2016) indicates that the total aerosol AOD and  
119 aerosol scattering albedo (SSA) in the lake areas of the YRD exceeded 0.6 and its single scattering  
120 albedo (SSA) was and ~0.88, respectively, in lake and urban areas of central to east YRD with  
121 significant seasonality, while in Hangzhou, they were larger than 0.72 and 0.89, respectively (Qi et al.,  
122 2016). In addition to east China, Che et al. (2011, 2013), Zhao et al. (2013), Zhu et al. (2014), Tao et al.  
123 (2014) and Yu et al. (2015) investigated the columnar aerosol optical properties in Waliguan Mt. area,  
124 Taklimakan Desert, industrial region of northeast China, north China (which can be taken as a region  
125 with the background aerosol), the Sichuan Basin in southwest China and desert region of northwest  
126 China, respectively. In 2015, Che et al. (2015a) initiated a systematic long term measurements of the  
127 countrywide AOD and AE in China from 2002 to 2013, including 4 remote sites, 25 rural sites, 21  
128 urban sites. Their results showed that annual mean AOD were 0.14, 0.74 and 0.54 at the rural sites, at  
129 the urban sites, and in east China, respectively. Zhuang et al. (2014a) indicates that a one-year observed  
130 AOD and AE of the total aerosols in urban area of Nanjing (urNJ, west YRD) was similar to Pan et al.  
131 (2010), but difference existed. In addition to Based on observed aerosol optical properties, the observed  
132 based aerosol direct radiative forcing (DRFs) were are also estimated around the world (such as:  
133 Markowicz et al., 2008; Khatri et al., 2009; Kuhlmann and Quaas, 2010; Alam et al., 2011, Zhuang et  
134 al., 2014a, and Xia et al., 2016). However, almost all of their investigations focused on the total aerosol

135 forcing. Markowicz et al. (2008) found that the daytime surface DRF exceeded  $-20 \text{ W/m}^2$  in the Persian  
136 Gulf. Khatri et al. (2009) indicated that aerosols had strong ability to absorb solar radiation in Nagoya  
137 in summer, resulting in a positive DRF of  $+2.5 \text{ W/m}^2$  at the top of the atmosphere (TOA) and a strong  
138 negative forcing of  $-71.8 \text{ W/m}^2$  at the surface. Alam et al. (2011) found that aerosols could lead to a  
139 decrease in the TOA solar radiative flux, with a mean value of  $-22 \text{ W/m}^2$  in Karachi. In East Asia or  
140 China, Kuhlmann and Quaas (2010) indicated that shortwave radiation was reduced by about  $25 \text{ W/m}^2$   
141 due to the total aerosols over Qinghai-Tibet Plateau. For example, Xia et al. (2016) stated that regional  
142 mean aerosol DRF in China was about  $-16 \sim -37 \text{ W/m}^2$  at the TOA and about  $-66 \sim -111 \text{ W/m}^2$  at the  
143 surface when solar zenith angle was about  $60^\circ$ .

144 Although considerable studies on the observed columnar aerosol optical properties ~~based~~  
145 ~~observations~~ have been carried out in China or even within YRD (one of the rapidest urbanization  
146 regions in China), there ~~are~~ still have gaps need to be improved in-for the current observations ~~network~~  
147 ~~in China over YRD (one of the rapidest urbanization regions in China)~~, especially in the urban areas of  
148 the region with intense human activities. In YRD or east China, most of the investigations on the  
149 aerosol optical properties were focused on the coast, lake and rural regions (Pan et al., 2010; Yu et al.,  
150 2011; Che et al., 2015a; Qi et al., 2016) of central to east YRD. And most of them only address the total  
151 aerosol optical properties (independent of modes and compositions) except Qi et al., (2016), who also  
152 made an introduction on the aerosol physical parameters and size fractional SSA in eastern coast city  
153 (Hangzhou, hereinafter short for urHZ) of YRD. There is about 300 km of urHZ away from west YRD.  
154 As implied in Zhang et al. (2012), aerosols are complicated in compositions and spatial distributions  
155 especially in fast developing regions (such as YRD). Thus, large differences of the aerosol optical and  
156 physical properties might exist to degrees among the sites within YRD. Additionally, none of

157 researches mentioned above have studied the aerosol DRFs. Some investigations on the columnar  
158 aerosols in west YRD (urNJ) have been carried out in Zhuang et al. (2014a), but significant issues (not  
159 considered in theirs) still need to be further addressed, such as the size fractional optical parameters and  
160 DRFs of different aerosol components, as well as the size fractional aerosol physical properties.  
161 Therefore, it's still necessary to make a more integrated investigation on the aerosol optical and  
162 physical properties, as well as their DRFs in YRD. In this study, the unaddressed issues in west or  
163 whole YRD region mentioned above will be all included based on the measurements of Cimel  
164 sun-photometer in urNJ, combined with a radiation transfer model (TUV, Madronich, 1993).  
165 Additionally, the aerosol types and mixings in the region will be further identified and discussed based  
166 on the relationships among the aerosol optical properties. Third, the observed aerosol profiles, which  
167 have not been considered before in YRD, are further used and discussed here to calculate the aerosol  
168 DRFs. It believes that the results here would be advantageous ~~To fill the gaps and to better further~~  
169 understand the ~~characteristics of aerosol optical properties and DRF~~ over urban areas in YRD east  
170 region of China. Also, they are helpful to improve the model performance on the aerosol and its climate  
171 effects in relevant regions. Because, first of all, the observed aerosol parameters could be used for data  
172 assimilation to obtain more accurate inputs (including initial conditions and air pollutant emissions) of  
173 the model (Jiang et al., 2013 and Peng et al., 2017). Second, a more precise aerosol refractive index and  
174 size distribution used in numerical models would yield a more reasonable aerosol loadings and DRFs  
175 (Ma et al., 2017). Third, both the aerosol optical properties and DRFs could be used to validate the  
176 simulations, ~~we investigate the aerosol optical and physical properties observed by Cimel sun~~  
177 photometer (CE-318, Holben et al., 1998), as well as the aerosol direct radiative forcing ~~calculated with~~  
178 a radiation transfer model TUV (Madronich, 1993) ~~combined with observed aerosol profiles and~~

~~surface albedo in Nanjing. The aerosol optical properties include: 1) the optical depths of the total, absorbing and scattering aerosols (AOD, AAOD, SAOD, respectively) and their corresponding values in fine and coarse modes (FAOD, FAAOD, FSAOD, CAOD, CAAOD, CSAOD, respectively), 2) the Ångström exponents of the total, absorbing and scattering aerosols (AE, AAE, SAE, respectively) as well as their corresponding values in fine and coarse modes (FAE, FAAE, FSAE, CAE, CAAE, CSAE, respectively), 3) single scattering albedo of the total, fine and coarse aerosols (SSA, FSSA, CSSA) and 4) refractive indexes of the aerosols. The aerosol physical properties include: 1) the volume size distributions of the aerosols, 2) The aerosol effective and mean radius as well as their volume concentrations in all, fine, and coarse modes ( $R_{\text{eff}}$ ,  $FR_{\text{eff}}$ ,  $CR_{\text{eff}}$ ,  $R_{\text{mn}}$ ,  $FR_{\text{mn}}$ ,  $CR_{\text{mn}}$ ,  $Vol$ ,  $FVol$ ,  $CVol$ , respectively).~~

The method is described in Section 2. Results and discussions are presented in Section 3, followed by Conclusions in Section 4.

## 2 Methodologies

### 2.1 Sampling station and instruments

The observation site (Urban Environmental Monitoring Station of Nanjing University) is located in the ~~Gulou district~~, downtown area of Nanjing City (~~hereinafter short for urNJ~~, 32.05° N, 118.78° E), ~~west YRD~~. It is built on the roof of a 79.3 m-tall building, around which there ~~are almost have~~ no higher ~~obstacles~~~~buildings~~ and ~~no~~ industrial pollution sources within a 30 km radius but there are several main roads with apparent traffic pollutions. ~~Detailed information of the site~~ ~~The sketch map of the site (not shown) and the corresponding climatic features are~~ available in ~~Figure 1~~ of Zhu et al.

201 (2012).

202 The columnar aerosol optical properties and physical characters at the site were ~~observed from~~  
203 ~~measurements using of~~ the Cimel sun photometer (CE-318, Holben et al., 1998) during the period from  
204 Apr 2011 to Feb 2014. Routine maintains and calibrations were made during the observation period.  
205 Due to the malfunctions of the instrument and the problems of data transmission, the data from May to  
206 Sep 2012 and from Aug to Dec 2013 are invalid and excluded. The wavelength dependent optical depth  
207 (AOD) and Ångström exponents (AE) of the total aerosols were directly measured by CE-318, while  
208 the following variables ~~are derived using the DOBVIC algorithm (Dubovik et al., 2000; 2006),~~  
209 including the aerosol size distributions, ~~fractionated mode dependent~~ (fine and coarse) aerosol effective  
210 radius ( $R_{\text{eff}}$ ), mean radius ( $R_{\text{mn}}$ ), volume concentrations (Vol), wavelength dependent size fractional  
211 ~~aerosol optical depth in fine (FAOD) and coarse (CAOD) modes of the scattering, absorbing and total~~  
212 ~~aerosols~~, aerosol single scattering albedo (SSA) ~~in different modes (fine and coarse), absorbing and~~  
213 ~~scattering aerosol optical properties in different modes~~, as well as wavelength dependent refractive  
214 indices, are derived from the DOBVIC algorithm Version 2 (Dubovik et al., 2000; 2006). ~~The This~~  
215 ~~DOBVIC~~ algorithm has been widely used by the Aerosol Robotic Network (AERONET) and the China  
216 Aerosol Remote Sensing Network (CARSNET) and the products have been used globally as  
217 introduced in Introduction due to their high accuracies. The errors for AOD, absorption AOD (AAOD),  
218 SSA is 0.01, 0.01 and 0.03, respectively (Yu et al., 2011; Li et al., 2015c). The errors of the fine and  
219 coarse aerosol SSA is 0.037 and 0.085, respectively (Xu, 2015). The error of the refractive index is  
220 0.04 for real part and 0.0025-0.0042 for imaginary part (Yu et al., 2011). And the error of the volume  
221 size distribution is less than 10% in peak regions while about 35% in valley region or interval region  
222 between fine and coarse modes (Yu et al., 2011). Detailed descriptions on CE-318 and the

223 corresponding observations in CARSNET are available in Li et al. (2015a) and Che et al. (2015a). For  
 224 comparison, 550 nm AODs and SSAs are calculated based on given AODs at other wavelengths and  
 225 AEs (Angstrom. 1929):

$$226 \quad AOD_{550nm} = AOD_{440nm} \times \left(\frac{550_{nm}}{440_{nm}}\right)^{-AE_{440/870nm}} \quad (1)$$

$$227 \quad AAOD_{550nm} = AAOD_{440nm} \times \left(\frac{550_{nm}}{440_{nm}}\right)^{-AAE_{440/870nm}} \quad (2)$$

$$228 \quad SSA_{550nm} = \frac{AOD_{550nm} - AAOD_{550nm}}{AOD_{550nm}} \quad (3)$$

229 To make a further comparison, the concurrent observations of surface total aerosol absorption  
 230 coefficient (AAC) and Ångström exponents (AAE) measured by a 7-channel Aethalometer (model  
 231 AE-31, Magee Scientific, USA, Hansen et al., 1984; Weingartner et al., 2003 and Arnott et al., 2005)  
 232 are used. Detailed calculation and correction of AAC at the site could be found in Zhuang et al. (2015).

233 In addition, monthly mean optical depth (AOD) and Ångström exponent (AE) of the total aerosols  
 234 from satellite of Moderate Resolution Imaging Spectroradiometer (MODIS) were used to assist the  
 235 analysis.

236 Based on observed wavelength dependent aerosol optical properties, the aerosol direct radiative  
 237 forcing (DRF) in Nanjing-urNJ is investigated using a radiation transfer model TUV (Madronich, 1993).  
 238 Only clear sky DRFs are addressed here because almost all of the measurements are carried out in free  
 239 sky condition. The solar component of the radiative transfer scheme in TUV follows the  $\delta$ -Eddington  
 240 approximation. In addition to the aerosol optical properties, surface albedo (Palancar and Toselli, 2004)  
 241 and the aerosol vertical profiles (Forster et al., 2007) might also have significant influences on DRF.  
 242 Thus, the wavelength dependent surface albedo from MODIS, the annual and seasonal mean aerosol  
 243 profiles from Cloud-Aerosol Lidar and Infrared Pathfinder Satellite Observations (CALIPSO) and

244 Polarization-Raman Lidar in Nanjing would be included when assessing the aerosol DRF ~~in clear sky~~  
245 ~~condition~~. The aerosol DRF in this study is defined as the difference in net shortwave radiative fluxes  
246 between including and excluding aerosol effects at the TOA ~~or and at the~~ surface. Gas absorptions in  
247 the atmosphere were set to be constant. The scattering aerosol's SSA was set to 0.9999 (similar to  
248 sulfate or nitrate, Li et al., 2015b) when calculating its DRF. DRF of the absorbing aerosols is derived  
249 from the differences between the total and the scattering aerosol DRFs.

250

### 251 **3 Results and discussions**

#### 252 **3.1 Optical properties of the aerosols**

253 In this section, 550 nm optical depth, single scattering albedo and 440 nm refractive indices of the  
254 aerosols are discussed as representatives for the temporal variations and frequency distributions of  
255 these three kinds of the aerosol optical ~~properties~~ parameters. In addition to the ~~total whole~~ mode  
256 aerosols, the size fractional both (fine and coarse ones), ~~as well as both~~ aerosol optical properties of  
257 different components (scattering and absorbing aerosols) are also discussed in this section. Therefore,  
258 there are altogether nine types of aerosols, including the total aerosols, total fine aerosols, total coarse  
259 aerosols, scattering aerosols, fine scattering aerosols, coarse scattering aerosols, absorbing aerosols,  
260 fine absorbing aerosols, and coarse absorbing aerosols.

261 Table 1 ~~summarizes~~ summary the statistics of the aerosol optical properties during the study period  
262 in Nanjing ~~NJ~~. The means ~~for the total, scattering and absorbing aerosols'~~ 550 nm optical depth (AOD)  
263 ~~at 550 nm, averaged for the entire period, of the total aerosols is are~~ 0.65, 0.61, and 0.04, respectively.  
264 ~~AAOD only accounts for about 6% to the totals and the scattering aerosols account for as large as about~~  
265 94%. Fine mode aerosol AODs (FAOD, FSAOD and FAAOD) accounts for 81.53%, 81.97% and

266 56.09% of the total AOD, scattering AOD (SAOD) and absorbing AOD (AAOD) in this wavelength,  
267 respectively, implying that coarse aerosols is more absorbing than the fine ones. 440/870 nm AE of the  
268 total, scattering and absorbing aerosols are about 1.20, 1.19, and 1.32, respectively. Fine aerosols have  
269 much larger AEs. ~~F AE, FSAE and FAAE are about 0.4-0.5, 0.5 and 0.4~~ larger than ~~AE, SAE and AAE,~~  
270 ~~respectively~~ the total aerosols. Overall, the absorbing aerosols have smaller sizes than the scattering  
271 ones in all modes, especially in coarse mode, which is consistent with the results of the surface aerosols  
272 at the site (Zhuang et al., 2017). Annual mean 470/660 AAE (from AE-31) and 450/635 nm SAE (from  
273 Nephelometer Model Aurora 3000) of the near surface aerosols are 1.58 and 1.32, respectively, at the  
274 site during the period from March 2014 to Feb 2016 (Zhuang et al., 2017). The mean 550 nm SSAs are  
275 0.93, 0.95 and 0.82 for the total, fine and coarse aerosols, respectively, further implying that the coarse  
276 aerosols have different compositions and have much stronger ability to absorb solar short wave  
277 radiation than the fine aerosols. Comparisons also indicate that surface aerosol (SSA=0.9 in Zhuang et  
278 al., 2017) is a little more absorption than the columnar aerosols in urNJ. Annual mean surface SSA at  
279 550 nm for the total aerosols is little smaller (0.9) than the column one. The mean 440 nm refractive  
280 index is about  $1.44+0.0084i$ . The table also implies that west YRD could suffer very serious particle  
281 pollutions.

282 Table 1

283

### 284 3.1.1 Seasonal variations of the aerosol optical properties

285 Figure 1 presents the monthly variations of 550 nm AOD (a), SAOD (b) and AAOD (c) as well as  
286 the contributions of their fine or coarse mode to the corresponding totals. Temporal variations of the  
287 total aerosol AOD is consistent with SAOD due to significantly large ratio of SAOD/AOD. AODs are



288 all considerably high in winter due to a more intense emission of the trace gases and particles  
289 (According to Zhang et al., (2009), anthropogenic emissions of trace gases and aerosols have  
290 substantially seasonal variations, low in summer but high in colder seasons especially in winter.  
291 Therefore, AODs, including the total, scattering and absorbing ones, are considerably large in winter.  
292 However, a long distance transported due to the effects of dust aerosols from north China in spring and  
293 high efficiencies of moisture absorption and scattering aerosol chemical transformation in summer (Li  
294 et al., 2015a), also lead to high AODs are also large in these two seasons. Additionally, gas to particle  
295 transformation might be more efficient in summer, which somewhat contribute to larger SAOD or  
296 FSAOD in this season. Overall, lower AODs are all found in fall for the total, scattering and absorbing  
297 aerosols. Therefore, dust episodes, relative humidity (RH) and chemical processes weaken the seasonal  
298 variation of total AOD purely induced by the emissions in urNJ, west YRD. tradeoff among  
299 anthropogenic emissions, dust aerosols, and relative humidity somewhat weakens the seasonal  
300 variations of the all mode aerosol optical depth, including AOD, SAOD and AAOD. Instead, these  
301 processes prominent the AOD seasonality of different aerosol types in different size segments.  
302 However, the seasonalities of fine and coarse aerosol AODs are very different from and much stronger  
303 than the total mode aerosols. The largest AODs appear in spring for coarse scattering and absorbing  
304 aerosols (for both scattering and absorbing ones) while the largest AODs in summer for the fine  
305 aerosols are found in summer ones in urNJ. The coarse aerosol AODs are lowest in summer or fall  
306 while for fine aerosol AODs, the minimum appears in spring. The figure also implies that the scattering  
307 aerosols might have different size distribution from the absorbing aerosols. The fine mode fraction rate  
308 is 0.83 (peaking at 0.97) for scattering aerosol while 0.56 (peaking at 0.83) for absorbing  
309 aerosol. Owing to this, contributions of fine or coarse aerosol AODs to the totals are different among

310 different months. The peaks of FAOD/AOD, FSAOD/SAOD, and FAAOD/AAOD appear in August,  
311 with a value of 0.96, 0.97, and 0.83, respectively, while the largest values of CAOD/AOD,  
312 CSAOD/SAOD, and CAAOD/AAOD appear in April, being 0.35, 0.32, and 0.64, respectively. In  
313 other words, the fine aerosols have different compositions from the coarse ones. The figure further  
314 suggests that the scattering or total aerosols are mostly composed by the fine particles (>80%) while  
315 the absorbing aerosols are composed, at the same level, by both fine (56%) and coarse (44%) particles  
316 in column atmosphere in Nanjing, reflecting more absorbing of the coarse aerosol than the fine one.

317

318 Figure 1

319

320 The aerosol Ångström exponents also have substantially seasonal variations, especially for the  
321 absorbing aerosols as illustrated in Figure 2, showing monthly AE, FAE, CAE, SAE, FSAE, CSAE,  
322 AAE, FAAE, and CAAE at 440/870 nm. Similar to AODs, the seasonality of the total aerosol AEs is  
323 similar to that for the scattering aerosols. However, the seasonalities of the total and scattering aerosols  
324 is less profound than those of absorbing aerosols. For each component (scattering or absorbing one),  
325 the seasonal variations of its fine and coarse AEs are well agree with each other. Both fine and coarse  
326 aerosol AEs are all being close to zero line in summer for scattering and absorbing aerosols possibly  
327 due to the effects of high relative humidity in this season (Zhuang et al., 2014a), implying that both fine  
328 and coarse mode aerosols have larger sizes in summer than in the other seasons. The monthly  
329 variations of FAAE and CAAE are similar to each other, small in summer and large in spring and  
330 winter, although their magnitudes are different (Figure 3). However, FSAE and CSAE are strongly  
331 anti-correlated. The whole mode AE of each aerosol type is determined by the both variations of AE in

332 ~~each mode and fine mode fraction. Therefore, the smallest seasonal variation of the total absorbing~~  
333 ~~aerosol-AE (AAE), to some degree, agrees with that of FAAE or CAAE; its minimum appears in~~  
334 ~~summer (0.74 in July) for the total absorbing aerosols while. However, CAAOD accounts for the most~~  
335 ~~to AAOD in spring, AAE values are smaller, closer to CAAE's in this season than in fall and winter.~~  
336 ~~The seasonality of SAE is different from both FSAE's and CSAE's; it is also different from AAE's.~~  
337 ~~Under the combined effect of FSAE and CSAE, SAE minimum appears in spring (0.94 in Mar) for the~~  
338 ~~total scattering aerosols while the larger ones are found in summer and fall. Similar to AAE but more,~~  
339 ~~the curve of SAE would move toward the sides of CSAE in spring while toward FSAE side in summer~~  
340 ~~because the peaks of CSAOD/SAOD and FSAOD/SAOD appears in spring times and in summer times,~~  
341 ~~respectively as shown in Figure 1. Similarly, the total aerosol AE is determined by the both variations~~  
342 ~~of each aerosol type's AE and fraction rate of the scattering (or absorbing) aerosol to the totals. Similar~~  
343 ~~to AOD, the seasonality of the total aerosol AEs is more consistent with that of the scattering aerosols.~~  
344 The figure also indicates that the ~~coarse~~-scattering aerosols have much larger sizes (~~negative values of~~  
345 ~~CSAE~~) than the ~~coarse~~-absorbing aerosols, especially in coarse mode, suggesting that the CSAE might  
346 ~~have much greater influence on the total SAE than CAAE on the total AAE, although the ratio of~~  
347 ~~CSAOD/SAOD is smaller than that of CAAOD/AAOD. Further comparison indicates that t~~The  
348 seasonal variations of columnar SAE and AAE are consistent with the ones of surface SAE and AAE  
349 (results not shown here) at the site.

350

351 Figure 2

352

353 In addition to AOD and AE, monthly variations of the aerosol single scattering albedo (SSA) and

354 refractive indices are also investigated as shown in Figure 3, ~~which shows the monthly variations of the~~  
355 ~~all, fine and coarse aerosol SSA at 550 nm and the total aerosol refractive indices at 440 nm.~~ SSA is  
356 affected by both scattering and absorbing aerosols, as well as their relative contributions. The fine  
357 particles are much more scattering than the coarse aerosols. ~~Furthermore~~ ~~However,~~ ~~CSSA~~ ~~the coarse~~  
358 aerosol SSA has more significant seasonality ~~than FSSA.~~ ~~The total aerosol single scattering albedo, i.e.,~~  
359 ~~SSA, is somewhere in between FSSA and CSSA depending on the ratios of FAOD to AOD.~~ Overall,  
360 both FSSA and CSSA are relative smaller in summer than in the other seasons although they are  
361 considerable large in August 2011, implying that the two types of aerosols in summer are more  
362 absorbing than in the other seasons. The total aerosol SSA is somewhere in between FSSA and CSSA  
363 depending on the ratios of FAOD to AOD and it has ~~However, SSA has a~~ different seasonal variation  
364 from FSSA or CSSA. SSA is the smallest in spring ~~Due due~~ to the largest contribution of coarse  
365 aerosols ~~in spring, SSA is the smallest in the season.~~ The aerosol refractive indices also show  
366 substantial seasonality. The real part is large in spring but small in summer, which is similar to what  
367 was observed in Taihu Lake in ~~the middle of~~ central YRD (Yu et al. 2011). The imaginary parts show  
368 relatively weaker seasonal variations than the real parts.

369

370 Figure 3

371

372 Table 2 summarizes the abovementioned seasonal means with the corresponding standard  
373 deviations for ~~all the~~ all aerosol optical properties ~~in the four seasons.~~ It provides more quantitative  
374 variations of the aerosol optical properties compared with the figures above. Seasonal mean 550 nm  
375 AOD, SAOD and AAOD vary from 0.59 in fall to 0.75 in summer, from 0.55 in fall to 0.70 in summer,

376 and from 0.037 in fall to 0.050 in spring, respectively. CAOD, CSAOD, CAAOD account for the  
377 majority of AOD, SAOD and AAOD in spring, with the ratios of 30.1%, 27.9%, and 58.1%,  
378 respectively. FAOD, FSAOD, FAAOD account for the majority of AOD, SAOD and AAOD in summer,  
379 with the ratios of 90.5%, 91.2% and 70.2%, respectively. As discussed above, the seasonal variations of  
380 the total mode aerosol AEs and SSA are different from the ones ~~in each mode of fine or coarse aerosol~~  
381 ~~AEs and SSA, respectively~~. The seasonal mean 440/870 nm ~~AE, SAE and AAE~~ vary from ~~0.99 in~~  
382 ~~spring to 1.37 in fall, from~~ 0.98 in spring to 1.38 in fall, and from 0.78 in summer to 1.50 in winter.  
383 Seasonal mean ~~SSA, FSSA and CSSA~~ vary ~~from 0.920 in spring to 0.938 in winter,~~ from 0.940 in  
384 summer to 0.956 in ~~winter, winter~~ and from 0.787 in summer to 0.834 in spring, respectively. The real  
385 part of the aerosol refractive index has relatively stronger seasonality than the imaginary part. Their  
386 largest values are all found in spring. ~~Seasonal mean real and imaginary parts range from 1.41 in~~  
387 ~~summer to 1.46 in spring and from 0.0080 in fall to 0.0084 in spring.~~ Comparisons indicate that ~~t~~The  
388 seasonal variation of ~~the optical properties AOD~~ is highly inhomogeneous spatially ~~even within the~~  
389 ~~same region such as in~~ YRD. As indicated in Che et al. (2015a) ~~and Qi et al. (2016)~~, the largest AOD  
390 was found in spring while the lowest one appeared in summer in ~~Hangzhou~~urHZ, ~~another city in~~  
391 ~~eastern coast east of~~ YRD. In Taihu Lake, ~~a rural site in central YRD,~~ the lowest AOD appeared in  
392 winter (Pan et al., 2010; Yu et al., 2011). ~~Additionally, the aerosols are the most absorbing in winter in~~  
393 ~~central regions of YRD (Taihu Lake and urHZ) and their SSA are as small as 0.88 (Yu et al., 2011 and~~  
394 ~~Qi et al., 2016). Aerosols in west YRD (urNJ) are more scattering than theirs and the smallest SSA~~  
395 ~~appears in spring during the sampling periods. The aerosols are more absorbing in winter (0.88) in~~  
396 ~~Taihu Lake (Yu et al., 2011) than in spring in urban Nanjing here (0.92).~~ ~~Nevertheless~~However, AEs  
397 ~~variations~~ are more consistency with each other among these sites, being smallest in spring and largest

398 in fall.

399 Table 2

400

### 401 3.1.2 Frequencies of the aerosol optical properties

402 All AODs and SSAs follow a near lognormal pattern and almost all of the AE and refractive  
403 indices follow a unimodal pattern (Figure 4). The ranges around their means dominated, accounting for  
404 at least 60% to their total data samples during the entire study period. Similar to the temporal variation,  
405 frequency distributions. In addition to the seasonal variations, frequency distributions of the  
406 abovementioned aerosol optical properties are also investigated. Figure 4 presents the frequencies of  
407 550-nm AOD, FAOD, CAOD, SAOD, FSAOD, CSAOD, AAOD, FAAOD and CAAOD in Nanjing  
408 during the entire study period. All AODs follow a near lognormal pattern. The curves of the total  
409 aerosols (Fig. 4a not shown) are also highly similar to the ones of scattering aerosols (Fig. b), at the  
410 same bandings, in both fine and coarse modes. The peaks of the frequency curves, all exceeding 30%,  
411 appear at the values between 0.3 and 0.5, 0.2 and 0.4, 0.04 and 0.08 for all and scattering aerosol AODs  
412 in all, fine and coarse modes, respectively. They appear at the values between 0.005 and 0.02, 0.005  
413 and 0.015, 0.005 and 0.01 for AAOD, FAAOD and CAAOD, respectively. The dominant ranges are  
414 from 0.3 to 0.9 for SAOD (AOD), 0.2 to 0.8 for FSAOD (SAOD) and 0.04 to 0.16 for CSAOD  
415 (CAOD), accounting for more than 83% (82%), 83% (82%), and 63% (67%), respectively, of the total  
416 data samples during the entire period. The dominating ranges are from 0.005 to 0.06 for AAOD, 0.005  
417 to 0.05 for FAAOD and 0.005 to 0.03 for CAAOD, accounting for more than 75%, 82% and 71%,  
418 respectively, of the total data samples during the entire period. The curves vary in different seasons (not  
419 shown here), shifting left ward in low AOD seasons and right ward in high AOD seasons as suggested

420 by Zhuang et al. (2015). In summer, the curves might even have two peaks for the scattering or total  
421 aerosols, which is similar to the observations in Taihu Lake (Yu et al., 2011). The frequency curve of  
422 the total AOD is much closer to that of fine AOD for scattering aerosols than for absorbing aerosols  
423 because FSAOD accounts for more than 82% of SAOD while FAAOD only accounts for 56% of  
424 AAOD.

425

426 Figure 4

427

428 — Due to the large ratio of the scattering aerosols to the total aerosols, the frequency of the total  
429 aerosol AEs resembles more that of the scattering aerosol AEs (Figures 5a and 5b). Almost all the AE  
430 frequencies follow a unimodal pattern, less sharply than those of the AODs in Figure 4. The dominant  
431 ranges are from 0.8 to 1.6 for SAE (AE), 1.3 to 2.1 for FSAE (FSAE) and 0.48 to 0.24 for CSAE  
432 (0.24 to 0.12 for CAE), accounting for more than 81% (83%), 83% (83%) and 82% (75%),  
433 respectively, of the total data samples during the entire period. The dominant ranges are from 0.8 to 1.8  
434 for AAE, 1.1 to 2.1 for FAAE and 0.6 to 1.6 for CAAE, accounting for more than 74%, 67% and 69%,  
435 respectively, of the total data samples during the entire period, implying a gentler curve of AAE than  
436 SAE. The frequencies of the absorbing aerosol AEs in different modes are different from those of the  
437 scattering aerosols ones (Figure 5b and 5c), so is FAAE and CAAE. The occurrences of smaller CAAE  
438 are relatively high. The values below 0.6 for CAAE account for more than 20% of the total data  
439 samples. In addition, however, the occurrences of the large FAAE and AAE exceeding 2.5 and 2.2 reach  
440 also has contributions (more than 5.4%) and 11%, respectively, implying again that the absorbing  
441 aerosols in fine mode have a few parts of finer particles. Both fine and coarse absorbing aerosols have

442 much smaller sizes than the scattering aerosols at the same modes. ~~The frequencies of AEs also have~~  
443 ~~substantial seasonality (not shown here). Comparing with the annual frequency of SAE, the peak of the~~  
444 ~~frequency shifts left ward in spring, from 0.8 to 1.0, but shift right ward in fall, from 1.4 to 1.6. The~~  
445 ~~frequency of AAE has a left ward shift in summer compared to the annual one, peaking at AAE values~~  
446 ~~between 0.6 and 0.8.~~

447

448 ~~Figure 5~~

449

450 ~~SSAs also follow a near lognormal pattern (Figure 6a). Frequency distribution of SSA also implies~~  
451 ~~that t~~The coarse aerosols are more absorbing than the fine aerosols ~~(Table 1 and Figure 3).~~  
452 Consequently, the frequencies of SSAs peaks ~~between 0.91 and 0.93,~~ between 0.95 and 0.97, and  
453 between 0.80 and 0.84 for the ~~ah,~~ fine, and coarse mode aerosols, respectively, in ~~Nanjing-urNJ~~ during  
454 the study period. ~~The dominant frequency appears from 0.89 to 0.97 for SSA, from 0.91 to 0.99 for~~  
455 ~~FSSA, and from 0.72 to 0.92 for CSSA, accounting for more than 75%, 87% and 78%, respectively, of~~  
456 ~~the total data samples during the entire study period. Fine aerosol~~ SSAs concentrates more in a narrow  
457 range (from 0.89 to 0.99) than CSSA (from 0.64 to 0.96). ~~Both real and imaginary parts of the aerosol~~  
458 ~~refractive index follow a unimodal pattern and they are fairly similar to each other (Figure 6b). For the~~  
459 ~~refractive index, t~~The frequencies peak between 1.39 and 1.42, and between 0.007 and 0.009 for the  
460 real and imaginary parts, respectively, in ~~Nanjing-urNJ~~ during the study period. ~~The prevailing~~  
461 ~~frequency ranges from 1.36 to 1.54 for the real part and from 0.003 to 0.013 for the imaginary,~~  
462 ~~accounting for more than 76% and 70% of the total data samples, respectively.~~

463 ~~The frequency patterns of the aerosol optical properties also have substantial seasonality (not~~



464 shown here). Overall, the curves would shift left-ward in low value seasons and right-ward in high  
465 value seasons. In summer, the AOD curves might even have two peaks for the scattering or total  
466 aerosols, which are similar to the observations in Taihu Lake (Yu et al., 2011). For SAE, the peak shifts  
467 left-ward in spring by 0.2, but right-ward in fall by 0.2. For SSA, ~~The seasonality of SSA frequency~~  
468 (not shown) indicates that both fine and coarse aerosol SSA frequencies have a left-ward shift in  
469 summer compared to the annual one, which is opposite to the frequency of the total SSA because the  
470 fine aerosol AODs dominate, accounting for about 91% of the totals. The real part frequency in spring  
471 has a significant right-ward shift compared to that in the entire study period, peaking between 1.46 and  
472 1.50 (not shown). The imaginary part frequency in winter has a significant left-ward shift compared to  
473 that in the study period, peaking between 0.001 and 0.003 (not shown).

474

475 **Figure 6**

476 

### 477 **3.1.3 Comparisons with MODIS AOD, AE and surface aerosols**

478 AOD and AE observed by CE-318 are in reasonable agreement with those from MODIS in  
479 seasonal variation and magnitude (Figure ~~75~~). The linear correlation coefficients are 0.75 and 0.86  
480 between CE-318 AOD and MODIS AOD and between CE-318 AE and MODIS AE, respectively. AOD  
481 at 550 nm from MODIS is larger than from CE-318, with an ~~averaged~~average value of 0.82 during the  
482 study period. The mean AE at 412/470 nm is about 1.43. The standard deviations of the AOD and AE  
483 are much larger from CE-318 than from MODIS possibly due to a higher temporal resolution of  
484 CE-318 observations.

485

486 | Figure [75](#)

487

488 | The columnar AAOD and AAE from CE-318 are fairly related to the surface aerosol absorption  
489 | coefficient (AAC) and AAE from AE-31 (Figure [86](#)). However, the relationship between AAOD and  
490 | AAC or between column and surface AAEs is worse than that between CE-318's and MODIS'.  
491 | Although surface aerosols could be affected by transport, it is mainly from local and regional emissions  
492 | and its loadings are highly related to the degree of the boundary layer development. As suggested by  
493 | Zhuang et al. (2014b and 2015), surface aerosol loadings are considerably low in afternoon and  
494 | summer times when the boundary layer are well developed. The columnar AAOD could additionally be  
495 | affected by the ~~upper aerosol~~ emissions and transportations in the upper atmosphere and it is less  
496 | affected by the boundary height compared with the surface AAC, thus contributing a relatively worse  
497 | relationship between AAOD and AAC. The surface AAE is more concentrated in a narrow range and it  
498 | is larger (1.6) than that from CE-318, implying that the surface absorbing aerosols are finer ~~thus-and~~  
499 | fresher. The linear correlation coefficients are 0.39 and 0.41 between AAOD and AAC and between  
500 | columnar and surface AAEs, which is slightly worse than those between FAAOD and AAC (0.46) and  
501 | between columnar FAAE and surface AAE (0.47).

502

503 | Figure [86](#)

504

### 505 | 3.1.4 Briefly discussions

506 | Ground based observed aerosols have much higher temporal resolutions compared with  
507 | satellite retrievals. The observed columnar optical properties could make up the deficiency of surface

508 aerosol data on one hand, and make us better understand the characteristics of the aerosols on the other  
509 hand. Additionally, they might be useful for improving the model performances on the aerosols and  
510 their radiative effects in YRD or east China. The observed aerosol parameters could be used for data  
511 assimilation, which can produce more accurate initial conditions of the model and variations of the  
512 aerosol emissions (Jiang et al., 2013 and Peng et al., 2017). The data set of the optical properties in  
513 most of the climate or air quality models are frequently from a given refractive index which is  
514 homogeneous in time and space. Therefore, a more precise aerosol refractive index used in numerical  
515 models would yield a more reasonable aerosol optical properties and radiative forcing in observed  
516 regions and around. Further, the observed aerosol optical properties could be also used to validate the  
517 simulations.

518 As mentioned in Introduction, mMost studies on the aerosol optical properties in China mainly  
519 focus on AOD and AE of the total aerosols in short term (i.e., episodes, Che et al., 2013; Zheng et al.,  
520 2016; Che et al., 2015b). Studies on annual (Yu et al., 2011) and decadal (Che et al., 2015a) scales have  
521 been carried out in recent years based on CE-318 measurements. Che et al. (2015a) indicated that long  
522 term averages of the total aerosol ~~optical depth~~AOD at 440 nm and ~~Ångström exponent~~AE at 440/870  
523 nm in urban areas were about 0.75 and 1.05 in north China, 0.98 and 1.09 in Sichuan Basin, 0.78 and  
524 1.36 in Pearl River Delta region (PRD), 0.65 and 1.0 in northeast China, 0.66 and 0.89 in northwest  
525 China, 0.92 and 1.0 in central China, 0.9 and 1.25 in coastal areas of YRD. The mean AOD at 440 nm  
526 in ~~urban Nanjing~~urNJ ~~averaged over the study period is about 0.84, which~~ is larger (0.84) than that in  
527 north~~ern~~ China, ~~northwest China, northeast China,~~ and PRD but smaller than that in coastal cities of  
528 YRD ~~and about the same as the one in HeFei (0.84)~~. Aerosols in northwestern and central China;  
529 central China, north China have larger sizes (smaller AE) than those in Nanjingwest YRD. ~~AE in the~~

530 ~~cities and at rural areas within YRD is at a similar magnitude.~~ Che et al. (2015a) further suggested that  
531 the aerosols in urban areas likely had larger AODs and AEs than those in mountain and desert areas, so  
532 did in ~~Nanjing~~urNJ. Qi et al. (2016) presents that the aerosol single scattering albedo at 440 nm in  
533 ~~urHZ~~Hangzhou, ~~east YRD~~ is about 0.90, 0.92 and 0.70 for the total, fine and coarse aerosols,  
534 respectively, also implying that the coarse aerosols are more absorbing than the fine ones. Our  
535 measurements show similar results to ~~Qi et al. (2016) for Hangzhou~~theirs. However, aerosols in  
536 ~~Nanjing~~urNJ are more scattering than in ~~Hangzhou~~urHZ in both fine and coarse modes, revealing  
537 inhomogeneous distributions of the aerosol compositions in YRD. Although some studies on the  
538 columnar aerosol optical properties based observations have been carried out in YRD (Pan et al., 2010;  
539 Yu et al., 2011; Zhuang et al., 2014a; Che et al., 2015a, Qi et al., 2016), study here further fill the gaps  
540 of the current observations. Based on authors previous research (Zhuang et al., 2014a), a more  
541 comprehensive and systematic analysis on the fractionated optical properties of different aerosols types  
542 are additionally carried out here. The results would be advantageous to further understand the aerosols  
543 over east China.

544

### 545 3.2 Physical properties of the aerosols

546 In addition to the optical properties, the aerosol physical properties including volume size  
547 distributions, mode dependent sizes (radius) and volume concentrations are also retrieved. Figure ~~9-7~~  
548 shows the volume size distributions of the aerosols in different seasons (Figure ~~9a7a~~) and in different  
549 AOD ~~(or polluted)~~ levels (Figure ~~9b7b~~) in ~~Nanjing~~urNJ. The figure shows that aAerosols in ~~Nanjing~~  
550 ~~urNJ~~urNJ have a typical bimodal structure in volume size distribution in all seasons, presenting a two-mode  
551 lognormal distribution: fine ~~mode~~(radius < 0.6  $\mu\text{m}$ ) and coarse mode (radius > 0.6  $\mu\text{m}$ ). Their annual

552 peaks appear at the radius of 0.148  $\mu\text{m}$  in fine mode and 2.94  $\mu\text{m}$  in coarse mode. Similar to the aerosol  
553 optical properties, aerosol volume size distribution also has substantial seasonality. Dust episodes lead  
554 to the peak value in spring is being much lower smaller in fine mode and higher than in coarse mode,  
555 which is opposite to than that in the other seasons (especially in summer), due to the effect of dusts  
556 which results in a left ward shift in the distribution in fine mode. Therefore, the mean radius of the  
557 aerosols increases significantly in spring due to a high proportion of coarse particles, leading to a  
558 smaller AE as discussed in precious sections. In summer, the curve has a right-ward shift, showing ~~an a~~  
559 ~~increase larger aerosol size~~ in both fine and coarse ~~aerosol sizes modes~~ due to high hygroscopic growth  
560 efficiency levels of moisture in the season. The fine particles dominate in summer and result in large AE,  
561 opposite to what is in spring. ~~In Nanjing, t~~ The aerosol volume size distribution varies with different  
562 AOD values (Figure ~~9b7b~~) in urNJ. Overall, the peaks ~~value likely has a substantial shift~~ right-ward  
563 ~~shift~~ with increasing AOD for fine aerosols ~~but while a slightly~~ left-ward ~~shift~~ for coarse aerosols,  
564 implying that the growth of the fine aerosols is advantageous to enhance the aerosol radiative effect. In  
565 urNJ, both fine and coarse particles basically have the same levels. The peaks are at the radii of 0.113  
566 and 3.857  $\mu\text{m}$  when AOD is below  $\sim 0.2-8$ . And the fine aerosols begin to dominate more and at 0.194  
567 and 2.94  $\mu\text{m}$  when AOD exceeds 0.81-4. Additionally, AOD show a positive dependence on the volume  
568 concentrations of both fine and coarse aerosols. The AOD in Nanjing could be evenly affected by both  
569 fine and coarse aerosols when AOD is considerably large or relatively small. High levels of AOD ( $>1.4$ )  
570 are attributed to the coarse aerosols in spring and to the fine aerosols in summer. AOD values ranging  
571 from 1.0 to 1.4 is more resulted from the fine particles. The results here are rather consistent with the  
572 ones in Yu et al. (2011), Qi et al. (2016), and Zheng et al. (2016). However, the figure here further  
573 reflects that both fine and coarse particles themselves could cause very serious haze pollutions in YRD.

574 leading to considerably high peaking values in both fine and coarse modes being found. This has not  
575 been observed in previous publications. The aerosol size distributions here are also very useful for  
576 optimizing numerical models. A more precise aerosol size distribution would make the models more  
577 accurate in describing the aerosol transportation, deposition as well as its radiative effects (Ma et al.,  
578 2017) in YRD or east China.

579

580 Figure 97

581

582 To further investigate the physical features, the seasonal variations in of the aerosol effective and  
583 mean radius, and as well as volume concentrations in Nanjing in urNJ are further presented in Figure 408.  
584 The mean effective radius are, which is generally smaller than the mean one in all modes, is about 0.34,  
585 0.16, and 2.18  $\mu\text{m}$  for the total, fine and coarse aerosols, respectively, during the study period. It  
586 additionally reflects that the aerosols in urNJ are dominated by the fine particles as discussed  
587 previously. The mean averaged radius are about 0.80, 0.19, and 2.67  $\mu\text{m}$  for the total, fine and coarse  
588 aerosols, respectively. The seasonal variation of the aerosol effective seasonal variations of the  
589 radiuses have a good anti-correlation to the one of AEs (Figure 2). resembles that of the mean radius in  
590 all the modes. Both fine and coarse aerosol radius are larger in summer than in the other seasons due to  
591 the moisture absorption growth of the aerosols. With seasonal variations in the proportion of fine or  
592 coarse aerosols in the total. However, the total aerosol radius of the total aerosols are is much larger in  
593 spring than in the other seasons due to a larger coarse fraction. The seasonal variations of the radius in  
594 all modes anti-correlate well with the corresponding aerosol AEs as shown in Figure 2. Different from  
595 the radius, the seasonal variations of the volume concentrations between fine and coarse aerosols are

596 ~~different, peaking in spring for coarse aerosol while in summer for fine aerosol. The mean volume~~  
597 ~~concentrations are 0.24, 0.11 and 0.13  $\mu\text{m}^3/\text{cm}^3$  for the total, fine and coarse aerosols during the study~~  
598 ~~period. Overall, Although both the fine and coarse aerosols have the same volume levelseventy~~  
599 ~~contribute to the total aerosol volume in NanjingurNJ annually, their contributions to the total aerosol~~  
600 ~~volumes vary significantly with seasons.similar to what is found in Hangzhou (Qi et al., 2016). The~~  
601 ~~coarse aerosols contribute slightly more to the total aerosol volume concentrations because of its high~~  
602 ~~proportions in spring (Figure 10b). The seasonality of the volume concentrations in fine and coarse~~  
603 ~~aerosols are different, although the seasonality of their radius are similar to each other, because the~~  
604 ~~volume also depends on the concentrations of the aerosols. The highest volume concentrations appear~~  
605 ~~in spring for the coarse aerosols and in summer the for fine aerosols. As expected, The coarse aerosol~~  
606 ~~directly leads to the largestseasonal variation of the total aerosol volume is affected by both fine and~~  
607 ~~coarse aerosolsvolume peaking in spring for the total aerosols.~~

608

609 Figure 408

610

### 611 3.3 Aerosol classification based on its optical properties

612 The aerosol ~~typesclusters, to a certain degree,~~ could be identified based on the relationships  
613 between SSA at 491 nm and AE at 491/870 nm, ~~between~~ real refractive index (RRI) at 670 nm and AE  
614 at 491/870 nm, as well as between SSA differences ( $d\text{SSA}=\text{SSA}_{870\text{nm}}-\text{SSA}_{491\text{nm}}$ ) and AE at 491/870 nm  
615 ~~as presented in (Russell et al., (2014), who as shown in Figure 11. Russell et al. (2014) proposed a~~  
616 ~~Mahalanobis Classification based on “a priori” information for each type aerosol source (e.g.: dust,~~  
617 ~~urban, biomass aerosols). Different aerosols then would mostly concentrate within the corresponding~~

618 ellipses of a two-dimensional scatter plot of SSA versus AE (or RRI versus AE, or dSSA versus AE).  
619 Based on their classification, the pure dust, polluted dust, biomass-burning, industrial urban,  
620 developing urban, marine aerosols (Figure 8 in Russell et al., 2014) all could be identified. ~~indicated~~  
621 ~~that~~For example: 1. The polluted dust aerosols would be mostly within the ellipses with~~have~~ smaller  
622 AE (near 1.0), relatively smaller SSA levels (0.85 to 0.95), but much larger real refractive index (1.45  
623 to 1.55) and SSA differences (0 to 0.05) compared with other aerosols. 2. The aerosols from the  
624 developing urban generally have smaller sizes than the polluted dust (AE ranging from 1 to 1.6), but  
625 they have larger SSA (0.9 to 1.0), smaller real refractive index (1.4 to 1.5) and SSA differences (around  
626 0). 3. The aerosols from the urban dominated by Industrial (UrbInd) or from biomass burning have the  
627 largest AE (exceeding 1.6). However, the UrbInd aerosols have much larger SSA and SSA differences  
628 while smaller real refractive index compared with biomass burning aerosols. ~~If there were two kind of~~  
629 ~~aerosols having nearly identical coordinates, further information is needed.~~ Based on their  
630 classification standards, aerosols in urNJ could basically be identified as the clusters of polluted dust,  
631 developing and industrial urban kinds during the sampling period as shown in Figure 9, which further  
632 supports the analysis in previous sections (Section 3). In spring, dusts emitted from the desert regions  
633 in northern or north of China ~~the Figure 11 presents that aerosols in urban area of Nanjing could be~~  
634 ~~effected by the long distant transported dust (or polluted dust) substantially in spring times in long~~  
635 distant arriving to YRD. During the transportation, trace gases or particles could be absorbed and then a  
636 heterogeneous chemical reaction occurs. And in ~~rest other~~ seasons, the aerosols are mostly from the  
637 local emissions within and they belong to the developing the urban areas and industrial areas around  
638 aerosols. Although urNJ is only about 300-400 km far away from the East China Sea, its aerosols are  
639 few composed by marine or sea salt components as illustrated in Figure 9. It is a pity that the



640 observations missed a biomass burning event in Jun 2012 (Zhuang et al., 2014b, 2015) when the  
641 instrument was maintained. Otherwise, the figure will be more comprehensive. It's a very serious  
642 biomass burning episode, which directly results in extremely high BC surface concentrations (6-7 times  
643 to the annual means, Zhuang et al., 2014b). Analysis here might further help us to understand the  
644 aerosol sources, transformations, transports and its radiative effects in YRD. And it Figure 11 would be  
645 more comprehensive if this event were captured. also indicates that the Mahalanobis Classification is  
646 a very useful approach for classifying the aerosol into types, especially in the cases of shortage of data  
647 or insufficient of methods. However, the method still has a limitation. The classified ellipses have some  
648 overlaps among different aerosols clusters. In overlap regions, it's hard to further identify the aerosol  
649 into types. For example, it's not easy to distinguish the polluted dust aerosol with large AE from the  
650 urban aerosols with smaller AE. Therefore, if there were two kinds of aerosols having nearly identical  
651 coordinates, further information is needed or more effective approaches should be taken into account.

652

653 Figure 11

654

655 In addition to the types, the aerosol mixtures/compositions could also be identified based on SSA  
656 and AAOD. Generally, dust aerosol has strong absorptions in ultraviolet (UV) band, but become  
657 non-absorbing in the visible band, leading to its and biomass burning aerosol SSAs increasing with  
658 wavelength monotonically. For biomass burning aerosol, its SSA would increase and decrease with  
659 wavelength, respectively monotonically. Non-monotonically changes variation in SSA with the  
660 wavelength might be due to the other type aerosol dominated mixtures as indicated by Li et al. (2015c),  
661 who then proposed two curvature parameters defined as the second derivative of the second-order

662 polynomial fit of SSA and wavelength and the fit of AAOD and wavelength as shown in Eq. 4 and Eq.  
663 5 to provide additional information on the aerosol compositions.

$$664 \quad \ln(SSA_{\lambda}) = \beta_2 \ln(\lambda)^2 + \beta_1 \ln(\lambda) + \beta_0 \quad (4)$$

$$665 \quad \ln(AAOD_{\lambda}) = \alpha_2 \ln(\lambda)^2 + \alpha_1 \ln(\lambda) + \alpha_0 \quad (5)$$

666 Where,  $-\beta_2$  and  $\alpha_2$  are the SSA Curvature and AADO Curvature, respectively. Detailed  
667 statements could be found in Li et al. (2015c). Based on these parameters, the aerosols could basically  
668 be identified as the dust dominated, black carbon (including biomass burning and urban/industrial  
669 aerosols) dominated and other mixed (peak) type aerosols. because the curvature probability (or  
670 frequency) distributions are different among different aerosol mixtures. The former two type of  
671 aerosols have monotonically increase and decrease SSA spectral shapes, respectively. As indicated in  
672 Li et al. (2015c), the SSA or AAOD Curvature is mostly concentrated at or around 0 for the BC  
673 dominated aerosol mixture, which is much smaller than that of dust dominated aerosol mixtures (0.1  
674 for SSA Curvature and 0.5-1 for AAOD Curvature) (Li et al., 2015c) over East Asia. Based on their  
675 method, the curvatures of SSA and AAOD are calculated and then divided into three categories  
676 according to the monotonicity of SSA. Results show that there are about 15.0%, 27.5% and 42.3%  
677 occurrences of monotonically increasing, decreasing and 670 nm peaking SSA spectrums, respectively,  
678 in urNJ. And their probability (or frequency) distributions are plotted in Figure 10. Both SSA and  
679 AAOD Curvatures have substantial seasonality, larger in colder seasons (not shown here). The figure  
680 indicates that Our observations show the similar results as shown in Figure 12 the SSA and AAOD  
681 curvature patterns are highly consistent with those in Li et al. (2015c) for the monotonic categories,  
682 which implying that there might be about 15% (mostly appearing in spring) and 27% (mostly being in  
683 fall and winter) occurrence of dust dominated and BC dominated mixing aerosols, respectively, in urNJ

684 during the observed period. For example, a very strong dust storm from northwest China and Mongolia  
685 (Li et al., 2015a) directly yielded mean SSA and AAOD Curvatures of 0.12 and 1.11, respectively, on  
686 1st May 2011, which are close to the values (0.11 and 1.24, respectively) of the pure dust aerosol (Li et  
687 al., 2015c). ~~— further implying that aerosols in urban Nanjing could be effected by the long distant~~  
688 ~~transported dust as indicated in Figure 11 and could also be affected by biomass burning or the~~  
689 ~~industrial emissions. The results additionally suggested that there are about 15% (mostly appearing in~~  
690 ~~Spring) and 27.5% (mostly being in Fall and Winter) occurrence of dust dominated and BC dominated~~  
691 ~~mixing aerosols, respectively, in urban areas of Nanjing during the observed period. For the rest~~  
692 ~~category with non-monotonic SSA spectrum, the SSA curvature are mostly concentrated from 0.3 to~~  
693 ~~0.8, implying that dust component might not exceed 10% while the scattering species (organic carbon~~  
694 ~~not included) at least accounting for 30% within the mixing particle in west YRD according to the~~  
695 ~~sensitive results in Li et al. (2015c). Subsidiary data are needed if more information were going to be~~  
696 ~~further identified. Results here might help us to better understand the mixings of the aerosols in urban~~  
697 ~~areas of YRD. Similar to the Russell et al. (2014), Li et al. (2015c) also provides an effective approach~~  
698 ~~to classify the aerosol compositions based on a single data set (such as the CE-318 retrievals).~~

699

700 Figure 4210

701

702 ~~— In May 2011, Nanjing was affected by a very strong dust storm from northwest China and~~  
703 ~~Mongolia (Li et al., 2015a), the mean SSA and AAOD Curvatures in 1st May 2011 were as large as~~  
704 ~~0.12 and 1.11, respectively, which is close to the values (0.11 and 1.24, respectively) of the pure dust~~  
705 ~~aerosol (Li et al., 2015c). Both SSA and AADO Curvatures have substantial seasonality, larger in~~

706 ~~colder seasons (not shown here).~~

707

### 708 3.4 The direct radiative forcing of the aerosols

709 Basing on abovementioned wavelength dependent optical properties and combining with the  
710 observed surface albedo and aerosol profiles, the ~~clear sky size fractional total, scattering and~~  
711 ~~absorbing~~-aerosol direct radiative forcing (DRF) ~~of different components in all, fine and coarse modes~~  
712 at both ~~the top of atmosphere (TOA)~~ and ~~the~~ surface in ~~Nanjing-urNJ~~ using are investigated using a  
713 radiation transfer model TUV (Madronich, 1993), ~~under clear sky condition~~. ~~Due to lacking SSA~~  
714 ~~observations of each aerosol component, t~~The scattering aerosol ~~DRF's SSA~~ is ~~estimated based on a~~  
715 ~~given SSA value (0.9999, assumed to be equaling~~ to that of sulfate or nitrate ~~aerosol) in reference,~~  
716 ~~which is about 0.9999 (Li et al., 2015b) when assessing its DRF. As indicated in last section, absorbing~~  
717 ~~aerosols in urNJ are always in a mixed state. Therefore, t~~The absorbing aerosol DRF ~~was is~~  
718 ~~inappropriate to be estimated directly using the BC SSA. Here, it is~~ derived from the difference  
719 between the total ~~aerosol~~ and scattering aerosol DRFs, ~~which might be more representativeness~~  
720 ~~because of lacking the observed SSA of the mixed absorbing aerosol. To make comparison, the aerosol~~  
721 ~~DRFs is also calculated~~ based on AAOs, AAEs and black carbon (BC) SSA (Li et al., 2015b) ~~is also~~  
722 ~~calculated to make a comparison with the absorbing aerosol DRFs.~~

723 ~~Observed aerosol profiles, which have not been used in previous investigation (e.g.: Zhuang et al.,~~  
724 ~~2014a), might be important to the DRFs estimating. Figure 13-11 shows the mean vertical aerosol~~  
725 ~~profiles of the aerosols~~ observed by CALIPSO ~~(annual scale data)~~ and Polarization-Raman Lidar ~~(PRL,~~  
726 ~~seasonal scale data)~~ in Nanjing. To make a comparison, ~~all~~ profiles in the figure have been standardized  
727 to the percentage (%). ~~Similar to AODs and AEs, the figure suggests that the ground and satellite based~~

728 ~~aerosol profiles also exist substantial differences. The CALIPSO profile is more homogeneous than the~~  
729 ~~PRL one. The aerosols mainly concentrate below 4 km, accounting for about 61% and 88%,~~  
730 ~~respectively. According to CALIPSO and Lidar, respectively, suggesting that differences exist~~  
731 ~~between CALIPSO and Lidar derived profiles and the vertical aerosols from the Lidar distribute much~~  
732 ~~more at the lower troposphere below 4 km. Due to lacking long-term measurement of PRL and the~~  
733 ~~different products among different observation platforms, both the CALIPSO and PRL profiles are used~~  
734 ~~here. Additionally, Thus, a combined profile (gray line) simply assumed to be averaged from between~~  
735 ~~CALIPSO and Lidar PRL (gray line) is additionally included. It indicates that aerosols account for~~  
736 ~~about 75% of the totals below 4 km and about 60% in the boundary layer for the combined profile,~~  
737 ~~which to some extent is similar to the default profile of TUV (Palancar and Toselli, 2004). The aerosol~~  
738 ~~DRFs would be all estimated by TUV using all these four profiles.~~

739

740 ~~Figure 13-11~~

741

#### 742 **3.4.1 The aerosol direct radiative forcing in both clear and cloudy sky conditions**

743 DRFs, unless otherwise specified, hereinafter all represent the averaged values among CALIPSO,  
744 ~~Lidar PRL~~ and combined profile based forcing ~~in clear sky condition~~. Figure ~~14-12~~ shows the seasonal  
745 ~~mean variations of the size fractional~~ daytime TOA and surface DRFs of the total, scattering and  
746 absorbing aerosols ~~in all, fine and coarse modes in clear sky conditions in urNJ Nanjing. The scattering~~  
747 ~~aerosol could exert a negative forcing both at TOA and the surface while the absorbing aerosol exerts a~~  
748 ~~positive forcing at TOA and a negative forcing at the surface.~~  
749 ~~—The aerosol DRFs are highly depended on the aerosol optical properties and compositions. Overall,~~

750 the fine aerosols have much more contributions to the total aerosol DRFs, especially for scattering  
751 aerosols. The coarse aerosol DRF is only ~15% of the fine aerosol DRF for scattering aerosols  
752 while >51% for absorbing aerosols at both the TOA and surface in urNJ. Negative scattering aerosol  
753 DRFs could be significantly offset at the TOA while further strengthened at the surface by absorbing  
754 aerosols. Therefore, the total coarse aerosol DRF at the TOA is very weak due to a much smaller CSSA  
755 and subsequently it has a much smaller contribution to the total aerosol DRF than the fine aerosols.  
756 Both the scattering and absorbing aerosol DRFs have similar ~~significant~~ seasonality to their AODs,  
757 peaking in summer for the total scattering aerosols while in spring for the total absorbing aerosols.  
758 However, the DRF seasonal variation of each aerosol type is consistent with each other within the  
759 same mode, strongest (weakest) forcing at TOA appears all peaking in summer (spring) for in fine mode  
760 while scattering aerosols and in spring (summer) for in coarse scattering aerosols mode. The fine  
761 scattering aerosol AOD is about one order of magnitude larger than the coarse one, directly resulting in  
762 its much stronger DRFs. In addition to SAODs, surface albedo ~~could~~ and the solar zenith angle also  
763 have influence on the variation of lead to changes in the aerosol DRFs. As implied in Zhuang et al.  
764 (2014a), in a brighter surface would yield a weaker negative DRF while a stronger positive DRF, the  
765 scattering aerosol DRFs might decrease in the condition with fixed loadings or AODs (Zhuang et al.,  
766 2014a). The seasonal mean surface albedo averaged from four wavelengths (440, 670, 870 and 1020  
767 nm) ~~are~~ is about 0.145, 0.170, 0.129, and 0.137 in spring, summer, fall, and winter, respectively,  
768 implying that the scattering aerosol DRFs, to some extent, are weakened in spring and summer due to  
769 the higher surface albedo. Therefore, the the strongest DRF for the total scattering aerosols DRF is  
770 stronger in winter than found in summer, orderly followed by that in winter, spring, although and fall  
771 due to the co-affections of SAODs and surface albedo, although SAOD in spring is lower/higher than

772 ~~that in winter. The seasonal variations in the surface scattering aerosol DRFs are consistent with those~~  
773 ~~at TOA.~~

774 ~~Similar to the scattering aerosols, the TOA DRFs of the absorbing aerosols are the strongest in summer~~  
775 ~~for fine mode and in spring for coarse mode when the aerosol AODs are the highest in the~~  
776 ~~corresponding seasons. However, the TOA DRFs are relatively weaker in winter for fine absorbing~~  
777 ~~aerosols and in summer and winter for coarse absorbing aerosols. Different from the scattering aerosols,~~  
778 ~~the coarse absorbing aerosol DRFs have the same orders of magnitude as the fine ones. DRFs of~~  
779 ~~absorbing aerosols are also affected by both the AAODs and surface albedo to a certain degree. Zhuang~~  
780 ~~et al. (2014a) stated that higher surface albedo would considerably lead to stronger TOA DRFs and~~  
781 ~~weaker surface DRFs for absorbing aerosols with fixed loadings or AAODs, which is different from the~~  
782 ~~scattering aerosols. Additionally, the solar zenith angle also plays a considerable role in intensifying~~  
783 ~~DRFs. For example, at 8 and 9 pm on 13th Aug in 2011, AAODs and AAEs are all equal to 0.23 and~~  
784 ~~1.18, respectively. However, the corresponding DRFs are 3.37 and 4.69 W/m<sup>2</sup> at TOA and 9.12 and~~  
785 ~~10.03 W/m<sup>2</sup> at the surface under a condition of the same SSA, surface albedo and aerosol profiles,~~  
786 ~~implying that the DRFs would be stronger in warmer seasons or at noon when the optical properties of~~  
787 ~~absorbing aerosols and the other affecting factors are fixed. Similarly, Thus, a stronger TOA DRF of~~  
788 ~~the fine absorbing aerosols in spring than in winter might be also related to higher surface albedo and~~  
789 ~~solar zenith angles, although their AAODs in winter are substantially higher. Both fine and coarse~~  
790 ~~absorbing aerosol DRFs at TOA are stronger in fall than in winter possibly owing to higher solar zenith~~  
791 ~~angles in fall. The all-mode absorbing aerosol DRFs at TOA also have different seasonality from the~~  
792 ~~scattering aerosols, being the strongest in spring, orderly followed by those in summer, fall and winter.~~  
793 ~~The seasonal variations of the absorbing aerosol DRFs at the surface are somewhat different from at~~

794 ~~TOA in fine and coarse modes.~~The weakest surface DRF appears in spring for fine absorbing aerosols  
795 and in summer for coarse absorbing aerosols possibly due to a higher surface albedo in this season ~~as~~  
796 ~~suggested by Zhuang et al. (2014a). The surface DRFs of the all-mode absorbing aerosols are also the~~  
797 ~~strongest in spring due to the combined effects of the corresponding fine and coarse aerosols.~~

798 ~~The absorbing aerosols can considerably offset the negative DRFs of the scattering aerosols at~~  
799 ~~TOA and strengthen the positive DRFs of the scattering aerosols at the surface (Figures 14a and~~  
800 ~~14d). Unlike the single aerosol type, the total aerosol DRFs are co-affected by both the scattering and~~  
801 ~~absorbing aerosols, meaning that the seasonal variation of the TOA DRF is additionally related to the~~  
802 ~~SSAs' seasonality.~~ Thus, the ~~weakest and~~ strongest TOA DRFs of the total fine aerosols appears in  
803 ~~spring and winter~~ instead of summer, respectively, and ~~t~~he total coarse aerosol DRFs ~~in summer~~ are  
804 positive at TOA in summer ~~due to a high proportion of absorbing aerosol to the totals (smaller SSA as~~  
805 ~~showed in Figure 3a).~~ For all modes, the seasonal variation of the total aerosol DRFs at TOA are more  
806 consistent with that of the fine mode, ~~and the DRFs are all weaker than the ones of scattering aerosols.~~  
807 Compared with the TOA DRFs of the total aerosols, ~~t~~he variations of surface DRFs ~~of the total fine~~  
808 ~~aerosols~~ are much more consistent with those of corresponding AODs, strongest in summer for fine  
809 aerosols while ~~the weakest~~ in spring for coarse aerosols, ~~which is opposite to the total coarse aerosols.~~  
810 ~~Due to the co-affected of fine and coarse aerosols,~~ ~~t~~he total aerosol DRFs ~~of all mode aerosols~~ at the  
811 surface are the strongest in summer and weakest in fall. ~~The existence of cloud would reduce the solar~~  
812 ~~radiation reaching the surface or lower atmosphere, thus affecting the aerosol DRFs, including their~~  
813 ~~levels and seasonality. This issue would be further addressed in the further.~~

814

815 Figure 1412



816

817 ~~To make comparison (Figure 13), Due to lack of the observed SSAs, the absorbing aerosol DRFs~~  
818 ~~here are mainly estimated from the difference between the total and scattering aerosol DRFs.~~  
819 ~~Additionally, absorbing aerosol~~ DRFs based on observed AAOD, AAE and fresh BC SSA (Li et al.,  
820 2015b) are also accessed ~~(named as the second way) to investigate the differences between these two~~  
821 ~~types of DRFs as shown in Figure 15.~~ Although the absorbing aerosol DRFs are estimated in different  
822 ways, they are highly correlated at both ~~the~~ TOA and ~~the~~ surface ~~as shown in the figure, implying that~~  
823 ~~they have the same seasonality.~~ ~~However~~Apparently, the DRFs from the second method are much  
824 weaker than that from the first one; ~~possibly due to the absorbing aerosol in urNJ being always in~~  
825 ~~mixed state as analysis in previous section or as indicated in Zhuang et al. (2015).~~ ~~implying that the~~  
826 ~~DRFs from these two methods might represent different mixing states of the absorbing aerosols.~~  
827 ~~Apparently, the second one represents the forcing of fresh absorbing aerosols while the DRFs from~~  
828 ~~the former one might represent the forcing of the aged or internally mixed absorbing aerosols.~~ Jacobson  
829 (2000) suggests that the aged (mixed) absorbing aerosols have much stronger ability to absorb solar  
830 radiation, with a factor of two. Zhuang et al. (2013a and 2013b) stated that the simulated regional mean  
831 TOA DRFs of the mixed BC (+1.56 W/m<sup>2</sup>) over East Asia is about 1.9 +1.56 W/m<sup>2</sup> for internally mixed  
832 BC and about +0.81 W/m<sup>2</sup> for times to that of none externally-mixed BC. And the ratio is about 1.73 in  
833 this study, implying that the absorbing aerosol DRF from the first way is reasonable. Comparison here  
834 further proves the importance of the mixing states to estimate the absorbing aerosol ~~direct~~ radiative  
835 ~~forcing effects.~~

836

837 Figure ~~15~~13

838

839 Table 3 lists the annual mean ~~clear-sky~~ size fractional DRFs of the total, scattering and absorbing  
840 aerosols ~~in all, fine and coarse modes~~ at both the TOA and ~~the~~ surface in Nanjing ~~NJ~~. The DRFs at the  
841 surface are all stronger than those at the TOA. The mean DRFs are -10.69, -16.45, 5.76 W/m<sup>2</sup> at TOA  
842 and -25.54, -21.37 and -8.38 W/m<sup>2</sup> at the surface for the total, scattering and absorbing aerosols,  
843 respectively. The TOA DRFs in fine mode are nearly an order of magnitude stronger than those in  
844 coarse mode for the total and scattering aerosols. The DRFs of the fine absorbing aerosols have the  
845 same orders of magnitude as, but stronger than those of the coarse absorbing aerosols.

846 Table 3

847

848 ~~—~~ Various studies on the aerosol DRFs have been carried out based on observations or  
849 numerical models. Over all, the DRFs of urban aerosols are much stronger than those on the regional or  
850 global scale. Forster et al. (2007) summarized the global mean clear ~~and cloudy~~ sky DRFs of the total  
851 aerosols from observations, ~~which are being~~ -5.4 ~~and~~ -0.55 W/m<sup>2</sup>, ~~respectively.~~ Zhuang et al. (2013a  
852 and 2013b) indicated a simulated clear sky DRFs being -4.97 W/m<sup>2</sup> for total aerosols while +1.2 W/m<sup>2</sup>  
853 for BC Using a regional climate chemistry model, RegCCMS, Zhuang et al. (2013a and 2013b)  
854 estimated the regional mean DRFs of the total and BC aerosols over East Asia and they are -4.97 and  
855 +1.2 W/m<sup>2</sup>, respectively, in clear sky. On a sub-regional or urban scale, observed based analysis  
856 showed that the total aerosol DRF always exceeded at least 10<sup>1</sup> W/m<sup>2</sup> (Markowicz et al., (2008; Khatri  
857 et al., 2009; Wang et al., 2009; Kuhlmann and Quaas, 2010; Alam et al., 2011; Che et al., 2015c, and so  
858 on). ~~found that the daytime surface DRF exceeded -20 W/m<sup>2</sup> in Persian Gulf. Khatri et al. (2009)~~  
859 ~~indicated that aerosols exerted a positive DRF of +2.5 W/m<sup>2</sup> at TOA and a strong negative forcing of~~

860 ~~-71.8 W/m<sup>2</sup> at the surface in Nagoya in summer. Alam et al. (2011) found that total aerosol DRFs at~~  
861 ~~TOA was about -22 W/m<sup>2</sup> in Karachi. In East Asia or China, Wang et al. (2009) reported that the TOA~~  
862 ~~DRFs of total aerosols in Beijing are -2, -21 and -16 W/m<sup>2</sup> on clear, haze, and fog days, respectively.~~  
863 Kuhlmann and Quaas (2010) ~~indicated~~ showed that the total aerosol DRFs was about -25 W/m<sup>2</sup> over  
864 Qinghai-Tibet Plateau. Che et al. (2014; 2015c) indicated that the daytime total aerosol DRFs in  
865 northeast China was about -16.82 W/m<sup>2</sup> while exceeded -30 W/m<sup>2</sup> in both the rural and urban areas of  
866 north China Plain in polluted episodes. Che et al. (2014) also reported that the TOA DRFs of the total  
867 aerosols in north China Plain exceeded -30 and -40 W/m<sup>2</sup> in rural and urban areas, respectively, during  
868 the period with serious haze fog episodes. Xia et al. (2016) pointed out that the regional mean DRF in  
869 China was about -16 ~ -37 W/m<sup>2</sup> at TOA and about -66 ~ -111 W/m<sup>2</sup> at the surface when solar zenith  
870 angle was about 60°. Over all, the DRFs of urban aerosols are much stronger than those on the regional  
871 ~~or global scale.~~ Our results show that aerosols in urban area of west YRD could also exert very strong  
872 DRF, as large as -25.5 W/m<sup>2</sup> at the surface. Apparently, the DRFs here would have smaller  
873 uncertainties than that from simulations because of the use of observations. Compared with the results  
874 in Zhuang et al. (2014a), DRFs here might be more precise because: 1. the observed aerosol profiles  
875 have not been used; and 2. the absorbed DRFs (might be underestimated) were calculated using fresh  
876 BC SSA in Zhuang et al. (2014a) same orders of magnitude of DRFs as those for other regions in earlier  
877 studies. This study further investigates the size fractional (fine and coarse) DRFs of different aerosol  
878 components in urban areas of west YRD, which is in favor of better understanding the acts of aerosols  
879 affecting solar short wave radiation. And these issues have not been addressed in previous researches.  
880 The results here could also be used to validate the numerical simulations to evaluate the model  
881 performance on the aerosol radiative effects.

882

883 **3.4.2 Sensitivity of t**~~The aerosol direct radiative forcing to varies in different~~ aerosol profiles

884 Different aerosol profiles might result in different DRFs. Figure ~~16-14~~ presents the TOA and  
885 surface DRFs of the ~~different aerosol types, including the total,~~ scattering, ~~and~~ absorbing aerosols ~~and~~  
886 ~~the totals,~~ based on four kinds of aerosol profiles from CALIPSO, ~~LidarPRL,~~ Combined CALIPSO and  
887 ~~Lidar-PRL~~ shown in Figure ~~13-11~~ as well as the default one in TUV (Palancar and Toselli, 2004) in  
888 clear sky condition. The figure shows that the aerosol ~~direct raidative forcing~~DRFs in clear sky  
889 ~~condition~~ is not very sensitive to the aerosol profiles, although the ~~differences among~~ absorbing aerosol  
890 TOA-DRFs ~~\_are more sensitive than scattering aerosols from different profiles are more obvious to~~  
891 ~~some degree than the scattering aerosol DRFs or the surface forcing.~~ Overall, both the scattering and  
892 ~~absorbing aerosol DRFs at TOA would become weaker to some extent if more aerosols were~~  
893 ~~concentrated in lower layers of atmosphere or within boundary layer especially for the latter one.~~ Here,  
894 a profile impact factor: PIF is defined as the ratio of the standard deviations among the four types of  
895 DRFs in Figure ~~16-14~~ to the averaged values among these four DRFs. The PIF is about 4.97% for  
896 absorbing aerosol TOA-DRF while below 2% for the rest types of DRFs ~~during the study period,~~  
897 ~~further proving the weak influence of the aerosol profile on the clear sky DRFs.~~ Overall, ~~both the~~  
898 ~~scattering and absorbing aerosol DRFs at TOA would become weaker to some extent if more aerosols~~  
899 ~~were concentrated in lower layers of atmosphere or within boundary layer especially for the~~  
900 ~~absorptions, implying that the aerosol profiles might also become significant in some extreme cases~~  
901 ~~(high level of aerosol appearing very low layers in serious pollution episodes).~~ ~~In contrast, t~~The aerosol  
902 profiles might have much more influence on the DRFs in cloudy sky condition because the absorbing  
903 aerosols over brighter cloud would absorb more short wave radiation (Podgorny and Ramanathan,

904 2001). This issue is also going to be addressed in the further.

905

906 Figure ~~46~~14

907

### 908 3.4.3 Briefly discussions

909 Although the observation based DRFs of the total, scattering and absorbing aerosols, as well as  
910 their sensitivities to the aerosol profiles are analyzed in this study; uncertainties still exist due to the  
911 measurement errors of the optical properties mentioned in Section 2. Additional estimations of the  
912 aerosol DRFs are carried out based on the errors of AOD, AAOD and SSAs. Results indicate that larger  
913 uncertainties of the aerosol DRFs are mainly derived from the errors of SSA or AAOD. Uncertainty of  
914 total aerosol AOD (0.01) only yield about 1% relative bias for the total aerosol DRFs at both the TOA  
915 and surface. The total or fine aerosol SSA error (0.03 or 0.037) may result in about 24% uncertainties at  
916 the TOA (<15% at the surface) to the corresponding DRFs. A larger coarse aerosol SSA error (0.085)  
917 leads to a ~24% uncertainties of its surface DRFs. AAOD errors (0.01) cause about 20% uncertainties  
918 to the absorbing DRFs at both the TOA and surface, while only 1.2% to the scattering DRFs. Overall,  
919 these uncertainties are relatively smaller than those presented in 5th IPCC report (IPCC, 2013) and they  
920 could be further decreased if the measurements or the algorithms were further improved. In addition to  
921 the uncertainties, this study ~~there~~ still exist limitations to be addressed in the future. First, the  
922 absorbing aerosol SSA should be further measured to better estimate corresponding DRFs ~~are estimated~~  
923 ~~from the difference between the total and scattering aerosol DRFs. The methods are still with~~  
924 ~~uncertainties to some extent. Therefore, the observed SSA of the absorbing aerosols is needed in further~~  
925 ~~studies to enhance the accuracy.~~ Second, the DRF would be a little more precise ~~uncertainty can be~~

926 ~~further reduced~~ if ~~data with the aerosols profiles with~~ higher temporal resolutions ~~of the aerosols~~  
927 ~~profiles are were~~ used ~~instead of to substitute~~ their annual means. Third, long-term trends of the aerosol  
928 optical properties and direct radiative forcing, including their interannual and interdecadal variations,  
929 should be taken into consideration. Finally, extremely high aerosol loadings are frequently observed in  
930 serious pollution episodes, including dust storms, biomass burning, and regional transport (Zhuang et  
931 al., 2014a, b and 2015). The aerosol optical and physical properties as well as the radiative forcing  
932 would be rather different in these extreme episodes, which also deserve further studies.

933

#### 934 4 Conclusions

935 In this study, the size fractional aerosol optical and physical properties observed by Cimel sun  
936 photometer (CE-318), as well as ~~its corresponding~~ direct radiative forcing (DRF) calculated by a  
937 radiation transfer model TUV based on ~~observationsed aerosol optical properties, profiles, and surface~~  
938 ~~albedo~~ in urban area of Nanjing (urNJ), west YRD, are investigated.

939 In urban area of west YRD, the annual mean total aerosol optical depths AOD at 550 nm are  
940 0.65, mostly contributed by the scattering components (0.61). The absorption fraction is as small as  
941 about ~6.7%, changing with the seasons, and 0.04 for the total (AOD), scattering (SAOD) and  
942 absorbing (AAOD) aerosols, respectively. There are about 80% of aerosols distributing in fine mode in  
943 urNJ during the sampling periods. The absorption fraction is about 4.6% in fine mode while 15.5% in  
944 coarse mode, showing a very different compositions and absorption characteristics of these two kinds  
945 of aerosols. The fine mode fractions of the total, scattering and absorbing aerosols are 81.53%, 81.97%  
946 and 56.09%, respectively. The absorbing aerosols are finer, with an Ångström exponent (AE) of 1.32 at  
947 440/870 nm, 0.13 (0.12) larger than the scattering (total) aerosols. Fine aerosol AEs are much larger

948 ~~than coarse one, especially for scattering aerosols. Additionally, the fine aerosol is more scattering~~  
949 ~~(SSA=0.95) while the coarse aerosol more absorption (SSA=0.82). The mean 440-nm refractive index~~  
950 ~~is about  $1.44+0.0084i$  during the study period. Compared with the satellite retrievals, the aerosol~~  
951 ~~optical properties here have much higher temporal resolutions and products AOD and AE observed by~~  
952 ~~CE 318 are rather similar to those from MODIS. AAOD and AAE from CE 318 to some extent are~~  
953 ~~related to the surface aerosol absorption coefficient (AAC) and AAE. The aerosols in Nanjing have~~  
954 ~~smaller AOD than, but the same AE as, and are more scattering than, those in coastal cities of YRD.~~  
955 ~~Further analysis on the aerosol optical properties indicates that there might be about 15% and 27%~~  
956 ~~occurrence of dust dominated and BC dominated mixing aerosols, respectively, in west YRD during the~~  
957 ~~observed period.~~

958       ~~The aerosol optical properties have significant seasonality. AOD and AE of scattering aerosols are~~  
959 ~~lowest in fall and in spring while highest in summer and fall, respectively. The highest AAOD and~~  
960 ~~AAE appear in spring and winter while the lowest ones are found in fall and summer. Fine mode AOD~~  
961 ~~are all at maximum in summer but minimum in spring, while coarse AOD are at maximum in spring.~~  
962 ~~The AEs in both fine and coarse modes are closer to zero in summer than those in the other seasons due~~  
963 ~~to the effects of high humidity. The total aerosol AOD and AE seasonality is consistent with the~~  
964 ~~scattering aerosols. However, the smallest SSA is found in spring, although both FSSA and CSSA are~~  
965 ~~relative smaller in summer. All AODs and SSAs follow a near lognormal pattern and almost all of the~~  
966 ~~AE and refractive indices follow a unimodal pattern. The ranges around their means dominated,~~  
967 ~~accounting for at least 60% to their total data samples during the entire study period. They also have~~  
968 ~~substantial seasonality.~~

969 ~~——~~The aerosols in west YRD~~Nanjing~~ have a two-mode lognormal pattern in volume size

970 distribution, ~~with substantial seasonality~~, peaking at the radius of 0.148 and 2.94  $\mu\text{m}$  in annual scale.  
971 ~~Both the fine and coarse particles have the same contribution to the totals at lower aerosol loadings~~  
972 ~~(AOD<0.8). In higher AOD (>0.8) levels, the fine aerosols are predominate. Results further indicate~~  
973 ~~that the fine or coarse aerosol could individually induce a very serious polluted episode in urban region~~  
974 ~~of west YRD. The fine (coarse) mode peak has a leftward (rightward) shift relative to the annual peaks~~  
975 ~~in spring while both of them have a right ward shift in summer. AOD show a positive dependence on~~  
976 ~~the volume concentrations in both fine and coarse modes. The peaks would be close to each other with~~  
977 ~~increasing AOD. Both the fine and coarse aerosols have the same level of volume concentrations,~~  
978 ~~although their mean effective radiuses differ by an order of magnitude of fine aerosol is an order of~~  
979 ~~magnitude smaller than the coarse one. The mean effective radius and volume concentrations of the all~~  
980 ~~modes are 0.34 $\mu\text{m}$  and 0.24  $\mu\text{m}^3/\text{cm}^3$ , respectively, all peaking in spring. It's well known that the~~  
981 ~~seasonality of the radius are anti-correlated well with the AEs.~~

982 The mean DRFs of the total aerosols are ~~is~~ -10.69, -16.45, -5.76  $\text{W}/\text{m}^2$  at the TOA and -25.54,  
983 ~~-21.37 and -8.38~~  $\text{W}/\text{m}^2$  at the surface for the total, scattering and absorbing aerosols, respectively, in  
984 clear sky condition. The fine mode aerosol DRFs at TOA accounts for more than 97% of the totals at  
985 the TOA are nearly an order of magnitude larger than the coarse ones for scattering aerosols while they  
986 have the same levels for absorbing aerosols. Estimations on the size fractional DRF of each aerosol  
987 component indicate that the coarse aerosol DRF is only ~15% of the fine one within scattering aerosols  
988 while >51% within absorbing aerosols at both the TOA and surface in urNJ. The DRFs estimated for  
989 urban NanjingurNJ in this study are much stronger than those on their regional or global scales means.

990 — The size fractional aerosol optical, physical properties and DRFs have significant seasonality  
991 in west YRD. The DRF variations of each aerosol type within the same mode are mostly consistent



992 with the variations of corresponding AODs, all peaking in summer for the fine aerosols while in spring  
993 for the coarse ones. However, the variations of total aerosol DRF at the TOA are different from  
994 corresponding AOD within the same size segment because negative DRFs of the scattering are always  
995 offset by absorbing aerosol. Both the fine and coarse aerosols have the largest size and are the most  
996 absorbing in summer, which are different from the whole mode aerosols (in spring). The seasonal  
997 variations of the DRFs, to some extent, are different between at TOA and the surface, between the  
998 scattering and absorbing aerosols, as well as between the fine and coarse modes. In clear sky condition,  
999 both the TOA and surface DRFs of scattering and absorbing aerosols are all the strongest in summer for  
1000 fine mode and in spring for coarse one. However, the largest DRF value appears in spring for total  
1001 scattering aerosols whereas in spring for total absorbing aerosols due to different fine mode fractions of  
1002 these two types of aerosols in different seasons, which further results in the strongest (weakest) DRFs  
1003 of all aerosols found in winter (spring) at the TOA and in summer (fall) at the surface due to different  
1004 fractions of scattering aerosols to the total aerosols.

1005 The ~~sensitivity~~ sensitivities of clear sky aerosol DRFs ~~on to~~ the aerosol profiles ~~is are~~ not  
1006 significant ~~in clear sky condition,~~ and the bias is all smaller than about 5% for the TOA DRFs of  
1007 ~~absorbing aerosol while less 2% for the rest DRFs.~~ Overall, both scattering and absorbing aerosol  
1008 DRFs at TOA would become a little weaker to some extent if more aerosols were concentrated in lower  
1009 layers of atmosphere ~~or within boundary layer,~~ especially for the absorbed DRFption. Further  
1010 investigation suggests that another uncertainty of the DRFs is from the measuring errors of the aerosol  
1011 optical properties. Larger biases are mainly from the errors of SSA and AAOD.

1012

1013 **Acknowledgements:** This work was supported by the National Key Basic Research Development

1014 Program of China ([2017YFC0209803](#), 2014CB441203, 2016YFC0203303), the National Natural  
1015 Science Foundation of China (41675143, 91544230, 41621005), ~~the New Teachers' Fund for~~  
1016 ~~Postdoctoral Fellows, Ministry of Education (20120091120031), FP7 project: REQUA~~  
1017 ~~(PIRSES-GA-2013-612671)~~, and a project Funded by the Priority Academic Program Development of  
1018 the Jiangsu Higher Education Institutions (PAPD). The authors would like to thank all members in the  
1019 AERC of Nanjing University for maintaining instruments.

1020

## 1021 **5 References**

1022 Alam, K., Trautmann, T., and Blaschke, T.: Aerosol optical properties and radiative forcing over  
1023 mega-city Karachi. *Atmos. Res.* 101, 773-782, 2011.

1024 Angström, A.: On the atmospheric transmission of sun radiation and on dust in the air, *Geogr. Ann.*, 11,  
1025 156–166, 1929.

1026 Arnott, W. P., Hamasha, K., Moosmuller, H., Sheridan, P. J., and Ogren, J. A.: Towards aerosol  
1027 light-absorption measurements with a 7-wavelength aethalometer: evaluation with a photoacoustic  
1028 instrument and 3-wavelength nephelometer, *Aerosol Sci. Tech.*, 39, 17–29,  
1029 doi:10.1080/027868290901972, 2005.

1030 Bellouin, N., Boucher, O., Tanré, D., and Dubovik, O.: Aerosol absorption over the clear-sky oceans  
1031 deduced from POLDER-1 and AERONET observations, *Geophys. Res. Lett.*, 30, 1748,  
1032 doi:10.1029/2003GL017121, 2003.

1033 Bergin, M. H., Cass, G. R., Xu, J., Fang, C., Zeng, L., Yu, T., Salmon, L. G., Kiang, C. S., Tang, X. Y.,  
1034 Zhang, Y. H., and Chameides, W. L.: Aerosol radiative, physical, and chemical properties in Beijing  
1035 during June 1999, *J. Geophys. Res.*, 106 (D16), 17969–17980, 2001.

1036 Cai, H. K., Zhou, R. J., Fu, Y. F., Zheng, Y. Y., and Wang, Y. J.: Cloud-aerosol lidar with or thogonal  
1037 polarization detection of aerosol optical properties after a crop burning case, *Clim. Environ. Res.*,  
1038 16, 469–478, 2011.

1039 Che, H. Z., Zhang, X. Y., Xia, X., Goloub, P., Holben, B., Zhao, H., Wang, Y., Zhang, X. C., Wang, H.,  
1040 Blarel, L., Damiri, B., Zhang, R., Deng, X., Ma, Y., Wang, T., Geng, F., Qi, B., Zhu, J., Yu, J., Chen,  
1041 Q., and Shi, G.: Ground-based aerosol climatology of China: aerosol optical depths from the China  
1042 Aerosol Remote Sensing Network (CARSNET) 2002–2013, *Atmos. Chem. Phys.*, 15, 7619–7652,  
1043 2015a.

1044 Che, H. Z., Zhao, H. J., Wu, Y. F., Xia, X. A., Zhu, J., Wang, H., Wang, Y. Q., Sun, J. Y., Yu, J., Zhang,  
1045 X. Y., and Shi, G. Y.: Analyses of aerosol optical properties and direct radiative forcing over urban  
1046 and industrial regions in Northeast China, *Meteorology and Atmospheric Physics*, 127(3), 345-354,  
1047 doi:10.1007/s00703-015-0367-3, 2015c.

1048 Che, H., Wang, Y., and Sun, J.: Aerosol optical properties at Mt. Waliguan observatory, China, *Atmos.*  
1049 *Environ.*, 45, 6004–6009, 2011.

1050 Che, H., Xia, X., Zhu, J., Li, Z., Dubovik, O., Holben, B., Goloub, P., Chen, H., Estelles, V.,  
1051 Cuevas-Agulló, E., Blarel, L., Wang, H., Zhao, H., Zhang, X., Wang, Y., Sun, J., Tao, R., Zhang, X.,  
1052 and Shi, G.: Column aerosol optical properties and aerosol radiative forcing during a serious  
1053 haze-fog month over North China Plain in 2013 based on ground-based sunphotometer  
1054 measurements, *Atmos. Chem. Phys.*, 14, 2125–2138, doi:10.5194/acp-14-2125-2014, 2014.

1055 Che, H., Xia, X., Zhu, J., Wang, H., Wang, Y., Sun, J., Zhang, X., and Shi, G.: Aerosol optical  
1056 properties under the condition of heavy haze over an urban site of Beijing, China, *Environ. Sci.*  
1057 *Pollut. R.*, 22, 1043–1053, doi:10.1007/s11356-014-3415-5, 2015b.

1058 Che, H., Wang, Y., Sun, J., Zhang, X., Zhang, X., and Guo, J.: Variation of Aerosol Optical Properties  
1059 over the Taklimakan Desert in China, *Aerosol Air Qual. Res.*, 13, 777–785, 2013.

1060 Chiang, C. W., Chen, W. N., Liang, W. A., Das, S. K., and Nee, J. B.: Optical properties of tropospheric  
1061 aerosols based on measurements of lidar, sun-photometer, and visibility at Chung-Li (25°N, 121°E),  
1062 *Atmos. Environ.*, 41, 4128–4137, doi:10.1016/j.atmosenv.2007.01.019, 2007.

1063 [Deng, J. J., Zhang, Y. R., Hong, Y. W., Xu, L. L., Chen, Y. T., Du, W. J., and Chen, J. S.: Optical](#)  
1064 [properties of PM<sub>2.5</sub> and the impacts of chemical compositions in the coastal city Xiamen in China,](#)  
1065 [Science of the Total Environment, 557-558, 665-675, 2016.](#)

1066 Dubovik, O. and King, M. D.: A flexible inversion algorithm for the retrieval of aerosol optical  
1067 properties from Sun and sky radiance measurements, *J. Geophys. Res.*, 105, 20673–20696,  
1068 doi:10.1029/2000JD900282, 2000.

1069 Dubovik, O., Sinyuk, A., Lapyonok, T., Holben, B. N., Mishchenko, M., Yang, P., Eck, T. F., Volten, H.,  
1070 Munoz, O., Veihelmann, B., van der Zande, W. J., Leon, J. F., Sorokin, M., and Slutsker, I.:  
1071 Application of spheroid models to account for aerosol particle nonsphericity in remote sensing of  
1072 desert dust, *J. Geophys. Res.-Atmos.*, 111, D11208, doi:10.1029/2005jd006619, 2006.

1073 Fan, X. H., Chen, H. B., Xia, X. A., Li, Z. Q., and Cribb, M.: Aerosol optical properties from the  
1074 Atmospheric Radiation Measurement Mobile Facility at Shouxian, China, *J. Geophys. Res.*, 115,  
1075 D00K33, doi:10.1029/2010JD014650, 2010.

1076 Forster, P., Ramaswamy, V., Artaxo, P., Berntsen, T., Betts, R., Fahey, D. W., Haywood, J., Lean, J.,  
1077 Lowe, D. C., Myhre, G., Nganga, J., Prinn, R., Raga, G., Schulz, M., and Van Dorland, R.: Changes  
1078 in atmospheric constituents and in radiative forcing, in: *Climate Change 2007: The Physical*  
1079 *Science Basis. Contribution of Working Group I to the Fourth Assessment Report of the*

1080 Intergovernmental Panel on Climate Change, edited by: Solomon, S. et al., Cambridge Univ. Press,  
1081 Cambridge, UK, 129–234, 2007.

1082 Hansen, A. D. A., Rosen, H., and Novakov, T.: The aethalometer: an instrument for the real time  
1083 measurements of optical absorption by aerosol particles, *Sci. Total Environ.*, 36, 191–196, 1984.

1084 He, X., Li, C. C., Lau, A. K. H., Deng, Z. Z., Mao, J. T., Wang, M. H., and Liu, X. Y.: An intensive  
1085 study of aerosol optical properties in Beijing urban area, *Atmos. Chem. Phys.*, 9, 8903–8915,  
1086 doi:10.5194/acp-9-8903-2009, 2009.

1087 Holben, B. N., Eck, T. F., Slutsker, I., Tanre, D., Buis, J. P., Setzer, A., Vermote, E., Reagan, J. A.,  
1088 Kaufman, Y. J., Nakajima, T., Lavenu, F., Jankowiak, I., and Smirnov, A.: AERONET-a federated  
1089 instrument network and data archive for aerosol characterization, *Remote Sens. Environ.*, 66, 1-16,  
1090 1998.

1091 Holler, R., Ito, K., Tohno, S., and Kasahara, M.: Wavelength-dependent aerosol single scattering albedo:  
1092 measurements and model calculations for a coastal site near the sea of Japan during ACE-Asia, *J.*  
1093 *Geophys. Res.*, 108, 8648, doi:10.1029/2002JD003250, 2003.

1094 [IPCC 2013: Climate Change 2013: The Physical Science Basis. Contribution of Working Group I to the](#)  
1095 [Fifth Assessment Report of the Intergovernmental Panel on Climate Change, edited by: Stocker, T.](#)  
1096 [F., Qin, D., Plattner, G.-K., Tignor, M., Allen, S. K., Boschung, J., Nauels, A., Xia, Y., Bex, V., and](#)  
1097 [Midgley, P. M., Cambridge University Press, Cambridge, UK and New York, NY, USA, 1535 pp.,](#)  
1098 [2013.](#)

1099 Jacobson, M. Z.: A physically based treatment of elemental carbon optics: implication for global direct  
1100 forcing of aerosols, *Geophys. Res. Lett.*, 27, 217-220, 2000.

1101 Jacobson, M. Z.: Control of fossil-fuel particulate black carbon and organic matter, possibly the most

1102 effective method of slowing global warming, *J. Geophys. Res.*, 107, 4410,  
1103 doi:10.1029/2001JD001376, 2002.

1104 [Jiang, Z., Liu, Z., Wang, T., Schwartz, C. S., Lin, H.-C., and Jiang, F.: Probing into the impact of](#)  
1105 [3DVAR assimilation of surface PM<sub>10</sub> observations over China using process analysis, \*J. Geophys.\*](#)  
1106 [Res. Atmos., 118, 6738–6749, doi:10.1002/jgrd.50495, 2013.](#)

1107 Khatri, P., Ishizaka, Y., and Takamura, T.: A study on aerosol optical properties in an urban atmosphere  
1108 of Nagoya, Japan. *J. Meteorol. Soc. Jpn.*, 87 (1), 19-38, 2009.

1109 Kiehl, J. T. and Briegleb, B. P.: The relative roles of sulfate aerosols and greenhouse gases in climate  
1110 forcing, *Science*, 260, 311–314, 1993.

1111 Kuhlmann, J., and Quaas, J.: How can aerosols affect the Asian summer monsoon? Assessment during  
1112 three consecutive pre-monsoon seasons from CALIPSO satellite data, *Atmos. Chem. Phys.*, 10,  
1113 4673-4688, doi:10.5194/acp-10-4673-2010, 2010.

1114 Li, J., Carlson, B. E., and Lacis, A. A.: Using single-scattering albedo spectral curvature to characterize  
1115 East Asian aerosol mixtures, *J. Geophys. Res. Atmos.*, 120, 2037–2052, 2015c.

1116 Li, J., Wang, W.-C., Liao, H., and Chang, W. Y.: Past and future direct radiative forcing of nitrate  
1117 aerosol in East Asia, *Theor. Appl. Climatol.*, 121, 445–458, 2015b.

1118 Li, S., Wang, T. J., Xie, M., Han, Y., and Zhuang, B. L.: Observed aerosol optical depth and angstrom  
1119 exponent in urban area of Nanjing, China, *Atmos. Environ.*, 123, 350-356,  
1120 doi:10.1016/j.atmosenv.2015.02.048, 2015a.

1121 Liao, H. and Seinfeld, J. H.: Global impacts of gas-phase chemistry-aerosol interactions on direct  
1122 radiative forcing by anthropogenic aerosols and ozone, *J. Geophys. Res.*, 110, D18208,  
1123 doi:10.1029/2005JD005907, 2005.

1124 [Ma, X. X., Liu, H. N., Liu, J., and Zhuang, B. L.: Sensitivity of climate effects of black carbon in China](#)  
1125 [to its size distributions, Atmospheric Research, 185, 118-130, 2017.](#)

1126 Ma, X., and Yu, F.: Effect of spectral dependent surface albedo on Saharan dust direct radiative forcing.  
1127 Geophys. Res. Lett. 39, L09808, 2012.

1128 Madronich, S.: UV radiation in the natural and perturbed atmosphere, In: Tevini, M. (Ed.), UV-B  
1129 Radiation and Ozone Depletion, Effects on Humans, Animals, Plants, Microorganisms, and  
1130 Materials, Lewis Publisher, Boca Raton, pp. 17-69, 1993.

1131 Markowicz, K. M., Flatau, P. J., Remiszewska, J., Witek, M., Reid, E. A., Reid, J. S., Bucholtz, Z., and  
1132 Hilben, B.: Observations and modeling of the surface aerosol radiative forcing during UAE. J.  
1133 Atmos. Sci. 65, 2877-2891, 2008.

1134 Menon, S., Hansen, J., Nazarenko, L., and Luo, Y. F.: Climate effects of black carbon aerosols in China  
1135 and India, Science, 297, 2250–2253, doi:10.1126/science.1075159, 2002.

1136 Palancar, G.G., and Toselli, B. M.: Effects of meteorology and tropospheric aerosols on UV-B radiation:  
1137 a 4-year study. Atmos. Environ. 18, 2749-2757, 2004.

1138 Pan, L, Che, H. Z., Geng, F. H., Xia, X. A., Wang, Y. Q., Zhu, C. Z., Chen, M., Gao, W., and Guo, J. P.:  
1139 Aerosol optical properties based on ground measurements over the Chinese Yangtze Delta Region,  
1140 Atmos. Environ., 44, 2587-2596, doi:10.1016/j.atmosenv.2010.04.013, 2010.

1141 [Peng, Z., Liu, Z. Q., Chen, D., and Ban, J. M: Improving PM2.5 forecast over China by the joint](#)  
1142 [adjustment of initial conditions and source emissions with an ensemble Kalman filter, Atmos. Chem.](#)  
1143 [Phys., 17, 4837–4855, 2017.](#)

1144 Penner, J. E., Andreae, M., Annegarn, H., Barrie, L., Feichter, J., Hegg, D., Jayaraman, A., Leaitch, R.,  
1145 Murphy, D., Nganga, J., and Pitari, G.: Aerosols, their direct and indirect effects, in: Climate

1146 Change 2001: The Scientific Basis. Contribution of Working Group I to the Third Assessment  
1147 Report of the Intergovernmental Panel on Climate Change, edited by: Houghton, J. T. et al.,  
1148 Cambridge University Press, Cambridge, UK and New York, NY, USA, 289–348, 2001.

1149 Podgorny, I. A., and Ramanathan, V.: A modeling study of the direct effect of aerosols over the  
1150 tropical Indian Ocean, *J Geophys. Res.* 106, D20, 24097–24105, 2001.

1151 Qi, B., Hu, D. Y., Che, H. Z., Du, R. G., Wu, Y. F., Xia, X. A., Zha, B., Liu, J., Niu, Y. W., Wang, H.,  
1152 Zhang, X. Y., and Shi, G. Y.: Seasonal variation of aerosol optical properties in an urban site of the  
1153 Yangtze Delta Region of China. *Aerosol Air Qual. Res.*, 16, 2884-2896, 2016.

1154 Reddy, M. S., Boucher, O., Bellouin, N., Schulz, M., Balkanski, Y., Dufresne, J. L., and Pham, M.:  
1155 Estimates of global multicomponent aerosol optical depth and direct radiative perturbation in the  
1156 Laboratoire de Meteorologie Dynamique general circulation model, *J. Geophys. Res.*, 110, D10S16,  
1157 doi:10.1029/2004JD004757, 2005.

1158 Russell, P. B., Kacenelenbogen, M., Livingston, J. M., Hasekamp, O. P., Burton, S. P., Schuster, G. L.,  
1159 Johnson, M. S., Knobelspiesse, K. D., Redemann, J., Ramachandran, S., and Holben, B.: A  
1160 multiparameter aerosol classification method and its application to retrievals from spaceborne  
1161 polarimetry, *J. Geophys. Res.-Atmos.*, 119, 9838–9863, doi:10.1002/2013JD021411, 2014.

1162 Sun, H., Pan, Z., and Liu, X.: Numerical simulation of spatial-temporal distribution of dust aerosol and  
1163 its direct radiative effects on East Asian climate, *J. Geophys. Res.*, 117, D13206,  
1164 doi:10.1029/2011JD017219, 2012.

1165 Tao, R., Che, H. Z., Chen, Q. L., Tao, J., Wang, Y. Q., Sun, J. Y., Wang, H., and Zhang, X. X.: Study of  
1166 aerosol optical properties based on ground measurements over Sichuan Basin, China, *Aerosol and*  
1167 *Air Quality Research*, 14: 905–915. doi:10.4209/aaqr.2012.07.0200, 2014.



1168 Wang, T. J., Zhuang, B. L., Li, S., Liu, J., Xie, M., Yin, C. Q., Zhang, Y., Yuan, C., Zhu, J. L., Ji, L. Q.,  
1169 and Han, Y.: The interactions between anthropogenic aerosols and the East Asian summer monsoon  
1170 using RegCCMS, *J. Geophys. Res. Atmos.*, 120, doi:10.1002/2014JD022877, 2015.

1171 Wang, Y., Che, H. Z., Ma, J. Z., Wang, Q., Shi, G. Y., Chen, H. B., Goloub, P., and Hao, X. J.: Aerosol  
1172 radiative forcing under clear, hazy, foggy, and dusty weather conditions over Beijing, China,  
1173 *Geophys. Res. Lett.*, 36, L06804, doi:10.1029/2009GL037181, 2009.

1174 Weingartner, E., Saathoff, H., Schnaiter, M., Streit, N., Bitnar, B., and Baltensperger, U.: Absorption of  
1175 light by soot particles: determination of the absorption coefficient by means of aethalometers, *J.*  
1176 *Aerosol Sci.*, 34, 1445–1463, doi:10.1016/S0021-8502(03)00359-8, 2003.

1177 Wu, Y. F., Zhang, R. J., Pu, Y. F., Zhang, L. M., Ho, K. F., and Fu, C. B.: Aerosol optical properties  
1178 observed at a semi-arid rural site in northeastern China, *Aerosol Air Qual. Res.*, 12, 503–514, 2012.

1179 Xia, X. A., Li, Z. Q., Holben, B., Wang, P., Eck, T., Chen, H. B., Cribb, M., and Zhao, Y. X.: Aerosol  
1180 optical properties and radiative effects in the Yangtze Delta region of China, *J. Geophys. Res.*, 112,  
1181 D22S12, doi:10.1029/2007JD008859, 2007.

1182 Xia, X., Che, H., Zhu, J., Chen, H., Cong, Z., Deng, X., Fan, X., Fu, Y., Goloub, P., Jiang, H., Liu, Q.,  
1183 Mai, B., Wang, P., Wu, Y., Zhang, J., Zhang, R., and Zhang, X.: Ground-based remote sensing of  
1184 aerosol climatology in China: aerosol optical properties, direct radiative effect and its  
1185 parameterization, *Atmos. Environ.*, 214, 243-251, doi:10.1016/j.atmosenv.2015.06.071, 2016.

1186 Xu, J., Bergin, M. H., Greenwald, R., Schauer, J. J., Shafer, M. M., Jaffrezo, J. L., and Aymoz, G.:  
1187 Aerosol chemical, physical, and radiative characteristics near a desert source region of Northwest  
1188 China during ACE-Asia, *J. Geophys. Res.*, 109, D19S03, doi:10.1029/2003JD004239, 2004.

1189 Xu, J., Bergin, M. H., Yu, X., Liu, G., Zhao, J., Carrico, C. M., and Baumann, K.: Measurement of

1190 aerosol chemical, physical and radiative properties in the Yangtze delta region of China, *Atmos.*  
1191 *Environ.*, 36, 161–173, 2002.

1192 Xu, J., Tao, J., Zhang, R., Cheng, T., Leng, C., Chen, J., Huang, G., Li, X., and Zhu, Z.: Measurements  
1193 of surface aerosol optical properties in winter of Shanghai, *Atmos. Res.*, 109-110, 25–35, 2012.

1194 [Xu, X.: Retrieval of aerosol microphysical properties from AERONET photolarimetric measurements.](#)  
1195 [PhD diss., Department of Earth and Atmospheric Sciences, University of Nebraska-Lincoln, 2015.](#)

1196 Yan, P., Tang, J., Huang, J., Mao, J. T., Zhou, X.J., Liu, Q., Wang, Z. F., and Zhou, H. G.: The  
1197 measurement of aerosol optical properties at a rural site in Northern China, *Atmos. Chem. Phys.*, 8,  
1198 2229–2242, doi:10.5194/acp-8-2229-2008, 2008.

1199 Yu, J., Che, H. Z., Chen, Q. L., Xia, X. A., Zhao, H. J., Wang, H., Wang, Y. Q., Zhang, X. X., and Shi,  
1200 G. Y.: Investigation of aerosol optical depth (AOD) and Ångström exponent over the desert region  
1201 of northwestern China based on measurements from the China Aerosol Remote Sensing Network  
1202 (CARSNET), *Aerosol Air Qual. Res.*, 15, 2024-2036, doi:10.4209/aaqr.2014.12.0326, 2015.

1203 Yu, X. N., Ma, J., Kumar, K. R., Zhu, B., An, J. L., He, J. Q., and Li, M.: Measurement and analysis of  
1204 surface aerosol optical properties over urban Nanjing in the Chinese Yangtze River Delta, *Sci. Total*  
1205 *Environ.*, 542, 277-291, 2016.

1206 Yu, X. N., Zhu, B., Yin, Y., Fan, S. X., and Chen, A. J.: Seasonal variation of columnar aerosol optical  
1207 properties in Yangtze River Delta in China, *Adv. Atmos. Sci.*, 28(6), 1326-1335,  
1208 doi:10.1007/s00376-011-0158-9, 2011.

1209 Zhang, L., Sun, J. Y., Shen, X. J., Zhang, Y. M., Che, H., Ma, L. Q., Zhang, Y. W., Zhang, X. Y., and  
1210 Ogren, J. A.: Observations of relative humidity effects on aerosol light scattering in the Yangtze  
1211 River Delta of China, *Atmos. Chem. Phys.*, 15, 8439–8454, 2015.

1212 Zhang, Q., Streets, D. G., Carmichael, G. R., He, K. B., Huo, H., Kannari, A., Klimont, Z., Park, I. S.,  
1213 Reddy, S., Fu, J. S., Chen, D., Duan, L., Lei, Y., Wang, L. T., and Yao, Z. L.: Asian emissions in  
1214 2006 for the NASA INTEX-B mission, *Atmos. Chem. Phys.*, 9, 5131–5153,  
1215 doi:10.5194/acp-9-5131-2009, 2009.

1216 Zhang, W., Hu, B., Chen, C. H., Du, P., Zhang, L., and Feng, G. H.: Scattering properties of  
1217 atmospheric aerosols over Lanzhou City and applications using an integrating nephelometer, *Adv.*  
1218 *Atmos. Sci.*, 21(6), 848–856, 2004.

1219 Zhang, X. Y., Wang, Y. Q., Niu, T., Zhang, X. C., Gong, S. L., Zhang, Y. M., and Sun, J. Y.:  
1220 Atmospheric aerosol compositions in China: Spatial/temporal variability, chemical signature,  
1221 regional haze distribution and comparisons with global aerosols, *Atmos. Chem. Phys.*, 12, 779–799,  
1222 doi:10.5194/acp-12-779-2012, 2012.

1223 Zhao, H. J., Che, H. Z., Zhang, X. Y., Ma, Y. J., Wang, Y. F., Wang, X. X., Liu, C., Hou, B., and Che,  
1224 X. C.: Aerosol optical properties over urban and industrial region of Northeast China by using  
1225 ground-based sun-photometer Measurement, *Atmos. Environ.*, 75, 270-278.  
1226 doi:10.1016/j.atmosenv.2013.04.048, 2013.

1227 Zheng, Y., Che, H. Z., Zhao, T. L., Xia, X. A., Gui, K., An, L. C., Qi, B., Wang, H., Wang, Y. Q., Yu, J.,  
1228 and Zhang, X. Y.: Aerosol optical properties during the World Athletics Championships and Victory  
1229 Day Military Parade over Beijing in August and September 2015, *Atmosphere*, 7(3), 47;  
1230 doi:10.3390/atmos7030047, 2016.

1231 Zhu, J., Che, H. Z., Xia, X. A., Chen, H. B., Goloub, P., and Zhang, W. X.: Column-integrated aerosol  
1232 optical and physical properties at a regional background atmosphere in North China Plain, *Atmos.*  
1233 *Environ.*, 84, 54-64, doi:10.1016/j.atmosenv.2013.11.019, 2014.

1234 Zhu, J., Wang, T., Talbot, R., Mao, H., Hall, C. B., Yang, X., Fu, C., Zhuang, B., Li, S., Han, Y., and  
1235 Huang, X.: Characteristics of atmospheric Total Gaseous Mercury (TGM) observed in urban  
1236 Nanjing, China, *Atmos. Chem. Phys.*, 12, 12103–12118, doi:10.5194/acp-12-12103-2012, 2012.

1237 Zhuang, B. L., Li, S., Wang, T. J., Deng, J. J., Xie, M., Yin, C. Q., and Zhu, J. L.: Direct radiative  
1238 forcing and climate effects of anthropogenic aerosols with different mixing states over China,  
1239 *Atmos. Environ.*, 79, 349–361, doi:10.1016/j.atmosenv.2013.07.004, 2013a.

1240 Zhuang, B. L., Liu, Q., Wang, T. J., Yin, C. Q., Li, S., Xie, M., Jiang, F., and Mao, H. T.: Investigation  
1241 on semi-direct and indirect climate effects of fossil fuel black carbon aerosol over China, *Theor.*  
1242 *Appl. Climatol.*, 114, 651–672, doi:10.1007/s00704-013-0862-8, 2013b.

1243 Zhuang, B. L., Wang, T. J., Li, S., Liu, J., Talbot, R., Mao, H. T., Yang, X. Q., Fu, C. B., Yin, C. Q.,  
1244 Zhu, J. L., Che, H. Z., and Zhang, X. Y.: Optical properties and radiative forcing of urban aerosols  
1245 in Nanjing, China, *Atmos. Environ.*, 83, 43–52, 2014a.

1246 [Zhuang, B. L., Wang, T. J., Liu, J., Li, S., Xie, M., Han, Y., Chen, P. L., Hu, Q. D., Yang, X. Q., Fu, C.](#)  
1247 [B., Zhu, J. L.: The surface aerosol optical properties in urban area of Nanjing, west Yangtze River](#)  
1248 [Delta, China, \*Atmos. Chem. Phys.\*, 17, 1143–1160, 2017.](#)

1249 Zhuang, B. L., Wang, T. J., Liu, J., Li, S., Xie, M., Yang, X. Q., Fu, C. B., Sun, J. N., Yin, C. Q., Liao, J.  
1250 B., Zhu, J. L., and Zhang, Y.: Continuous measurement of black carbon aerosol in urban Nanjing of  
1251 Yangtze River Delta, China, *Atmos. Environ.*, 89, 415–424, 2014b.

1252 Zhuang, B. L., Wang, T. J., Liu, J., Ma, Y., Yin, C. Q., Li, S., Xie, M., Han, Y., Zhu, J. L., Yang, X. Q.,  
1253 and Fu, C. B.: Absorption coefficient of urban aerosol in Nanjing, west Yangtze River Delta, China,  
1254 *Atmos. Chem. Phys.*, 15, 13633–13646, 2015.

1255

1256 **Figure captions:**

1257 Figure 1. Monthly variations of the total (a), scattering (b), and absorbing (c) aerosol optical depths  
1258 (AOD) at 550 nm, including the ratio of the AOD in fine or coarse mode to the AOD in all mode (line  
1259 with triangle markers in green) in urban area of Nanjing. The 10th, 25th, median, 75th, 90th percentile  
1260 values of the all mode AOD are presented as box plots. The monthly means of the all mode AODs are  
1261 presented as cycle markers in gray.

1262 Figure 2. Monthly variations of the total (a), scattering (b), and absorbing aerosol (c) Ångström  
1263 exponents (AE) at 440/870 nm for the all, fine and coarse modes in urban area of Nanjing.

1264 Figure 3. Monthly variations of the all, fine, and coarse mode aerosol single scattering albedo (SSA) at  
1265 550 nm (a) and the aerosol refractive indices at 440 nm (b) in urban area of Nanjing.

1266 Figure 4. Frequency distributions of the ~~total (a), scattering (b), and absorbing aerosol (c) size~~  
1267 ~~dependent~~ AODs at 550 nm (a), AEs at 440/870 nm (b), SSAs at 550 nm (c) as well as the real and  
1268 imaginary parts at 440 nm (c) ~~for the all (AOD, SAOD, AAOD), fine (FAOD, FSAOD, FAAOD) and~~  
1269 ~~coarse (CAOD, CSAOD, CAAOD) modes~~ in urban area of Nanjing.

1270 ~~Figure 5. Frequency distributions of the total (a), scattering (b), and absorbing aerosol (c) AEs at~~  
1271 ~~440/870 nm for the all (AE, SAE, AAE), fine (FAE, FSAE, FAAE) and coarse (CAE, CSAE, CAAE)~~  
1272 ~~modes in urban area of Nanjing.~~

1273 ~~Figure 6. Frequency distributions of the all (SSA), fine (FSSA), and coarse (CSSA) mode aerosol SSAs~~  
1274 ~~at 550 nm (a) and the real and imaginary parts at 440 nm (b) in urban Nanjing.~~

1275 Figure ~~7~~5. Comparisons between CE-318 and MODIS based AOD at 550 nm and between AE at  
1276 440/870 nm for CE-318 and at 412/470 nm for MODIS in Nanjing.

1277 Figure ~~8~~6. Comparisons between the absorbing aerosol optical depth (AAOD) at 550 nm from CE-318

1278 and surface absorption coefficient (AAC) at 520 nm from AE-31 (a) and between the column AAE at  
1279 440/870 nm from CE-318 and surface AAE at 470/880 nm from AE-31 (b) in urban Nanjing.

1280 Figure 97. The averaged aerosol volume size ( $\mu\text{m}^3/\mu\text{m}^2$ ) distributions in different seasons (a) and in  
1281 different AOD levels in urban Nanjing.

1282 Figure 108. Seasonal variations of the effective (a,  $\mu\text{m}$ ) and mean (b,  $\mu\text{m}$ ) radius of aerosols as well as  
1283 the aerosol volume concentrations (c,  $\mu\text{m}^3/\text{cm}^3$ ) in the all, fine and coarse modes in urban Nanjing.

1284 Figure 119. Relationships between the monthly mean values of 491 nm SSA and total Ångström  
1285 exponent (AE) at 491/870 nm (a), between the monthly mean values of the real refractive index at 670  
1286 nm and AE at 491/870 nm (b), and between the monthly mean values of the SSA difference (870–491  
1287 nm) and AE at 491/870 nm (c).

1288 Figure 1210. Distribution of the SSA and AAOD Curvatures in urban area of Nanjing under different  
1289 spectral SSA conditions, including monotonically decreasing, increasing SSA spectra and peaked SSA  
1290 spectra.

1291 Figure 1311. The aerosol vertical proportions (%) from CALIPSO, Polarization-Raman Lidar and their  
1292 average in Nanjing.

1293 Figure 1412. Seasonal variations of the clear sky aerosol direct radiative forcing (DRF,  $\text{W}/\text{m}^2$ ) at both  
1294 TOA (a~c) and the surface (d~f). The DRFs of the total (a, d), scattering (b, e) and absorbing (c, f)  
1295 aerosols in the all, fine and coarse modes are all investigated in urban Nanjing.

1296 Figure 1513. Comparisons in the absorbing aerosol DRFs ( $\text{W}/\text{m}^2$ ) between from BC SSA and from the  
1297 total aerosol DRF minus the scattering one.

1298 Figure 1614. Sensitivities of the TOA and the surface aerosol DRFs (day time,  $\text{W}/\text{m}^2$ ) to the different  
1299 aerosol profiles in clear conditions, for the total, scattering and absorbing aerosols.

1300

1301 **Tables:**

1302 Table 1 Statistical summary of the columnar aerosol optical properties in urban area of Nanjing

Factors	Max	Min	Mean±SD	Median
550 nm AOD	2.3208	0.2723	0.6494±0.2852	0.5912
550 nm FAOD	2.2216	0.1468	0.5257±0.2806	0.4479
550 nm CAOD	0.9891	0.0139	0.1237±0.1076	0.0858
550 nm SAOD	2.2744	0.2443	0.6059±0.2747	0.5492
550 nm FSAOD	2.1459	0.1435	0.5014±0.2713	0.4263
550 nm CSAOD	0.8842	0.0113	0.1045±0.0957	0.0705
550 nm AAOD	0.2304	0.0020	0.0435±0.0240	0.0421
550 nm FAAOD	0.1424	0.0005	0.0244±0.0175	0.0208
550 nm CAAOD	0.1163	0.0009	0.0192±0.0145	0.0156
440/870 nm AE	1.9100	0.3085	1.2045±0.2856	1.2436
440/870 nm FAE	2.3625	0.3565	1.7083±0.2979	1.7364
440/870 nm CAE	-0.0789	-0.3805	-0.1876±0.0430	-0.1898
440/870 nm SAE	1.9916	0.2958	1.1976±0.3085	1.2386
440/870 nm FSAE	2.3653	0.3463	1.7102±0.2980	1.7368
440/870 nm CSAE	-0.1048	-0.7111	-0.3838±0.1017	-0.3864
440/870 nm AAE	3.4619	0.1483	1.3237±0.4820	1.2587
440/870 nm FAAE	4.5118	0.2912	1.7521±0.6470	1.6516
440/870 nm CAAE	3.1264	-0.0844	0.8748±0.4589	0.8209
550 nm SSA	0.9959	0.8053	0.9297±0.0335	0.9305
550 nm FSSA	0.9974	0.8388	0.9524±0.0261	0.9549
550 nm CSSA	0.9835	0.5898	0.8208±0.0754	0.8225
440 nm Real part	1.6000	1.3300	1.4423±0.0638	1.4374
440 nm Imaginary part	0.0301	0.0005	0.0084±0.0047	0.0078

1303

AOD: Aerosol optical depth

1304

FAOD: Fine aerosol optical depth

1305

CAOD: Coarse aerosol optical depth

1306

SAOD: Scattering aerosol optical depth

1307

FSAOD: Scattering aerosol optical depth in fine mode

1308

CSAOD: Scattering aerosol optical depth in coarse mode

1309

AAOD: Absorbing aerosol optical depth

1310

FAAOD: Absorbing aerosol optical depth in fine mode

1311

CAAOD: Absorbing aerosol optical depth in coarse mode

1312

AE: Ångström exponent of total aerosols

1313

FAE: Ångström exponent of fine aerosols

1314

CAE: Ångström exponent of coarse aerosols

1315

SAE: Ångström exponent of scattering aerosols

1316

FSAE: Ångström exponent of scattering aerosols in fine mode

1317

CSAE: Ångström exponent of scattering aerosols in coarse mode

1318

AAE: Ångström exponent of absorbing aerosols

1319

FAAE: Ångström exponent of absorbing aerosols in fine mode

1320

CAAEE: Ångström exponent of absorbing aerosols in coarse mode

1321

SSA: Single scattering albedo of total aerosols

1322

FSSA: Single scattering albedo of fine aerosols

1323

CSSA: Single scattering albedo of coarse aerosols

1324

1325

Table 2 Seasonal mean±SD of the columnar aerosol optical properties in urban area of Nanjing

Factors	MAM	JJA	SON	DJF
550 nm AOD	0.6788±0.2919	0.7508±0.3749	0.5866±0.2447	0.6560±0.2976
550 nm FAOD	0.4739±0.2613	0.6798±0.3793	0.5149±0.2462	0.5687±0.2978
550 nm CAOD	0.2048±0.1356	0.0710±0.0599	0.0717±0.0346	0.0873±0.0685
550 nm SAOD	0.6284±0.2835	0.7031±0.3728	0.5495±0.2342	0.6157±0.2829
550 nm FSAOD	0.4529±0.2552	0.6463±0.3760	0.4901±0.2366	0.5428±0.2846
550 nm CSAOD	0.1756±0.1225	0.0568±0.0497	0.0593±0.0315	0.0728±0.0601
550 nm AAOD	0.0503±0.0208	0.0477±0.0307	0.0372±0.0200	0.0403±0.0271
550 nm FAAOD	0.0211±0.0125	0.0335±0.0212	0.0248±0.0157	0.0259±0.0211
550 nm CAAOD	0.0292±0.0165	0.0142±0.0137	0.0124±0.0066	0.0144±0.0111
440/870 nm AE	0.9915±0.2385	1.2174±0.2639	1.3744±0.1907	1.3134±0.2461
440/870 nm FAE	1.7474±0.2896	1.4701±0.3075	1.7408±0.2582	1.6935±0.3019
440/870 nm CAE	-0.1998±0.0352	-0.1699±0.0471	-0.1862±0.0424	-0.1807±0.0464
440/870 nm SAE	0.9812±0.2687	1.2733±0.2950	1.3824±0.2043	1.2956±0.2697
440/870 nm SFAE	1.7555±0.2862	1.5218±0.3397	1.7492±0.2545	1.6809±0.3039
440/870 nm SCAE	-0.3752±0.0743	-0.2815±0.0678	-0.3797±0.0991	-0.4016±0.1162
440/870 nm AAE	1.1885±0.4500	0.7971±0.2657	1.3290±0.4533	1.5007±0.4520
440/870 nm FAAE	1.7352±0.6059	0.9943±0.2672	1.6715±0.5970	1.8947±0.6545
440/870 nm CAAE	0.8542±0.4665	0.3771±0.2753	0.8312±0.4479	0.9798±0.4235
550 nm SSA	0.9204±0.0313	0.9241±0.0422	0.9348±0.0331	0.9378±0.0331
550 nm FSSA	0.9527±0.0237	0.9405±0.0356	0.9518±0.0253	0.9555±0.0265
550 nm CSSA	0.8340±0.0628	0.7868±0.0953	0.8115±0.0752	0.8211±0.0810
440 nm Real part	1.4647±0.0628	1.4075±0.0609	1.4252±0.0602	1.4404±0.0582
440 nm Imaginary part	0.0084±0.0040	0.0083±0.0052	0.0080±0.0044	0.0083±0.0053

1326

1327 Table 3. The annual mean aerosol direct radiative forcing ( $W/m^2$ ) in urban area of Nanjing

Species	Clear sky	
	TOA	Surface
TA	-10.69±3.37	-25.54±2.83
FA	-11.17±3.09	-21.37±2.78
CA	-0.33±0.60	-6.15±2.90
SA	-16.45±2.81	-17.17±2.96
FSA	-15.08±3.18	-15.74±3.35
CSA	-2.31±1.18	-2.42±1.24
AA	5.76±1.27	-8.38±1.56
FAA	3.91±0.95	-5.63±1.16
CAA	1.99±1.07	-3.73±1.71

1328

TA: Total aerosols

1329

FA: Fine aerosols

1330

CA: Coarse aerosols

1331

SA: All scattering aerosols

1332

FSA: Scattering aerosols in fine mode

1333

CSA: Scattering aerosols in coarse mode

1334

AA: All absorbing aerosols' forcing



1335

FAA: Fine absorbing aerosols' forcing

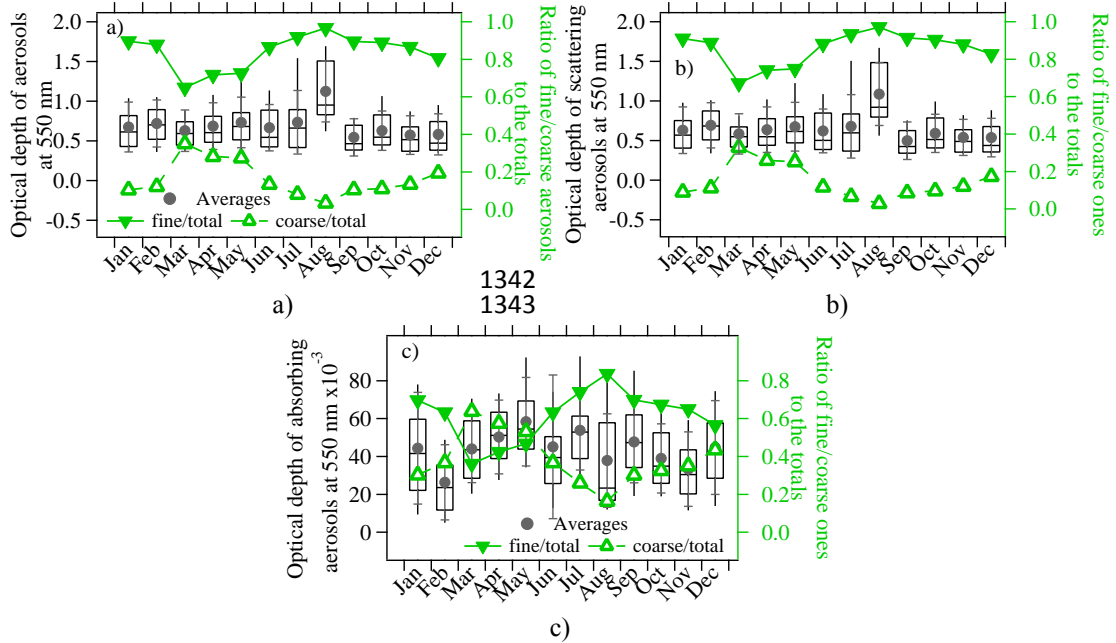
1336

CAA: Coarse absorbing aerosols' forcing

1337

1338

1339 **Figures:**

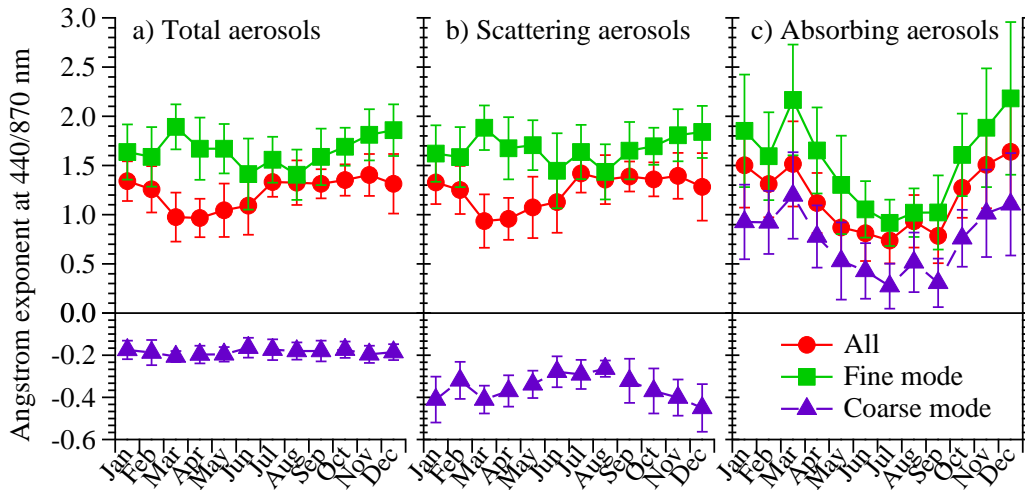


1340  
1341

1342  
1343

1344  
1345  
1346  
1347

Figure 1.



1348  
1349  
1350

Figure 2.

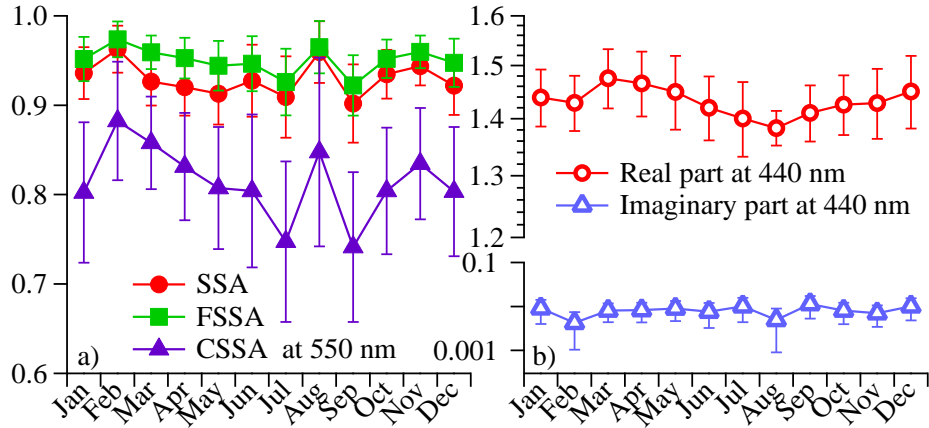
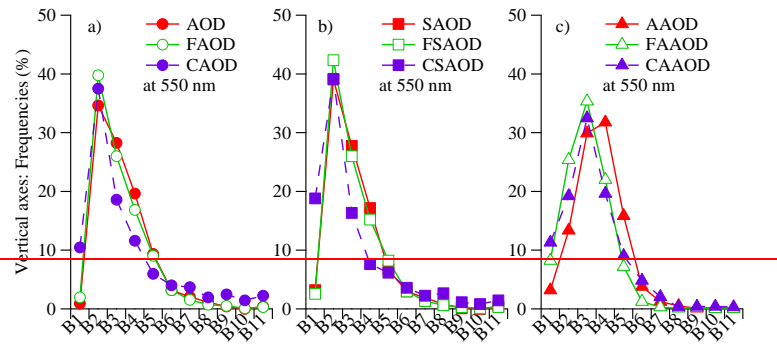


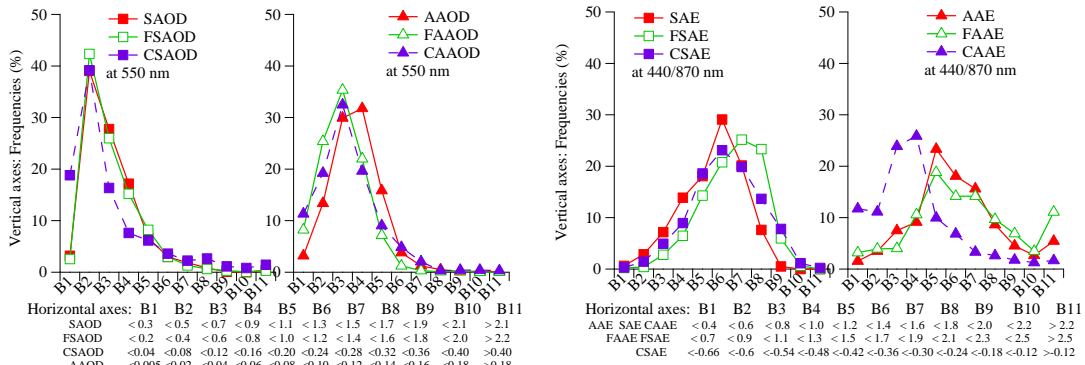
Figure 3

1351  
1352  
1353



Horizontal axes:	B1	B2	B3	B4	B5	B6	B7	B8	B9	B10	B11
AOD	<0.3	<0.5	<0.7	<0.9	<1.1	<1.3	<1.5	<1.7	<1.9	<2.1	>2.1
FAOD	<0.2	<0.4	<0.6	<0.8	<1.0	<1.2	<1.4	<1.6	<1.8	<2.0	>2.2
CAOD	<0.04	<0.08	<0.12	<0.16	<0.20	<0.24	<0.28	<0.32	<0.36	<0.40	>0.40
SAOD	<0.3	<0.5	<0.7	<0.9	<1.1	<1.3	<1.5	<1.7	<1.9	<2.1	>2.1
FSAOD	<0.2	<0.4	<0.6	<0.8	<1.0	<1.2	<1.4	<1.6	<1.8	<2.0	>2.2
CSAOD	<0.04	<0.08	<0.12	<0.16	<0.20	<0.24	<0.28	<0.32	<0.36	<0.40	>0.40
AAOD	<0.005	<0.02	<0.04	<0.06	<0.08	<0.10	<0.12	<0.14	<0.16	<0.18	>0.18
FAAOD	<0.005	<0.015	<0.03	<0.05	<0.07	<0.09	<0.11	<0.13	<0.15	<0.17	>0.17
CAAOD	<0.005	<0.01	<0.02	<0.03	<0.04	<0.05	<0.06	<0.07	<0.08	<0.09	>0.10

1354



Horizontal axes:	B1	B2	B3	B4	B5	B6	B7	B8	B9	B10	B11
SAE	<0.4	<0.6	<0.8	<1.0	<1.2	<1.4	<1.6	<1.8	<2.0	<2.2	>2.2
FSAE	<0.4	<0.6	<0.8	<1.0	<1.2	<1.4	<1.6	<1.8	<2.0	<2.2	>2.2
CSAE	<0.7	<0.9	<1.1	<1.3	<1.5	<1.7	<1.9	<2.1	<2.3	<2.5	>2.5
AAE	<0.66	<0.6	<0.54	<0.48	<0.42	<0.36	<0.30	<0.24	<0.18	<0.12	>0.12
FAAE	<0.4	<0.6	<0.8	<1.0	<1.2	<1.4	<1.6	<1.8	<2.0	<2.2	>2.2
CAAEE	<0.7	<0.9	<1.1	<1.3	<1.5	<1.7	<1.9	<2.1	<2.3	<2.5	>2.5

1355

1357

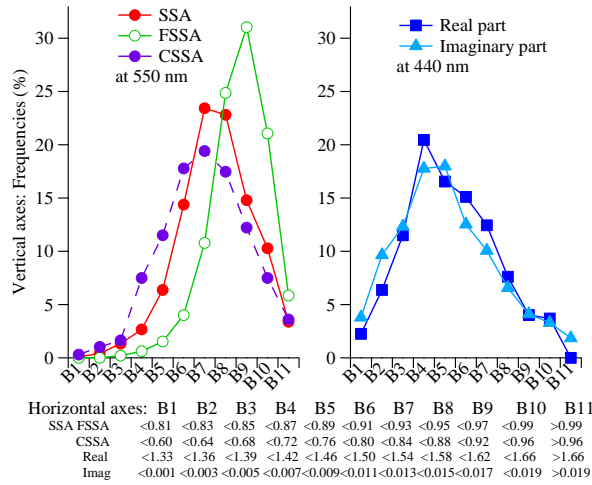
1356

a)

1358

b)

1359  
1360  
1361  
1362



e)  
Figure 4

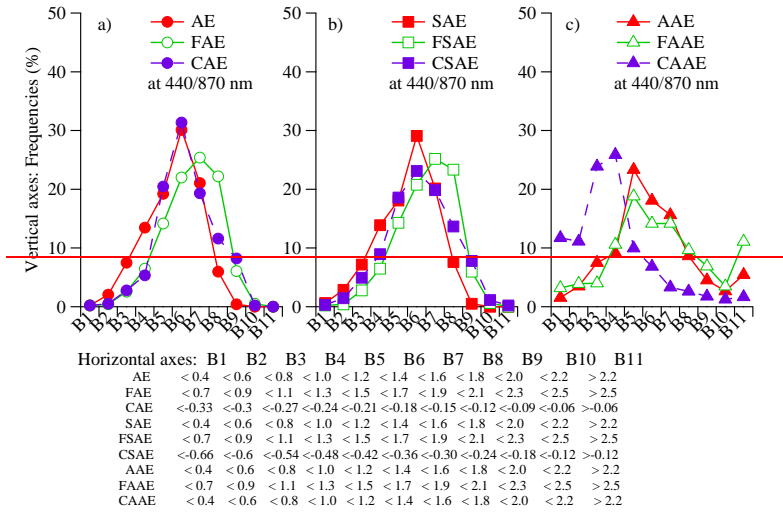
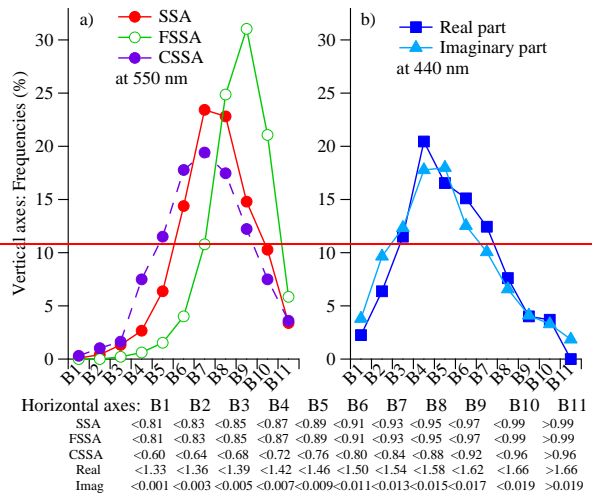


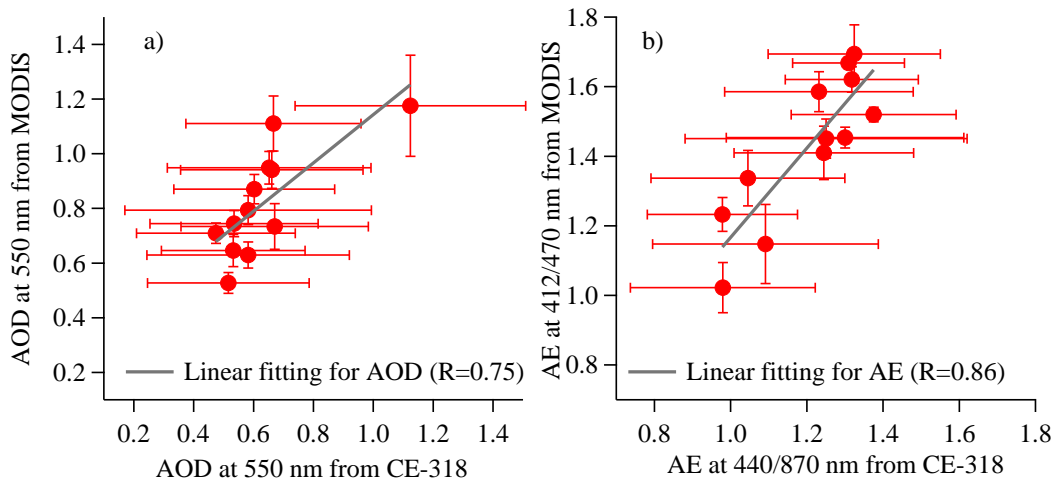
Figure 5



1366

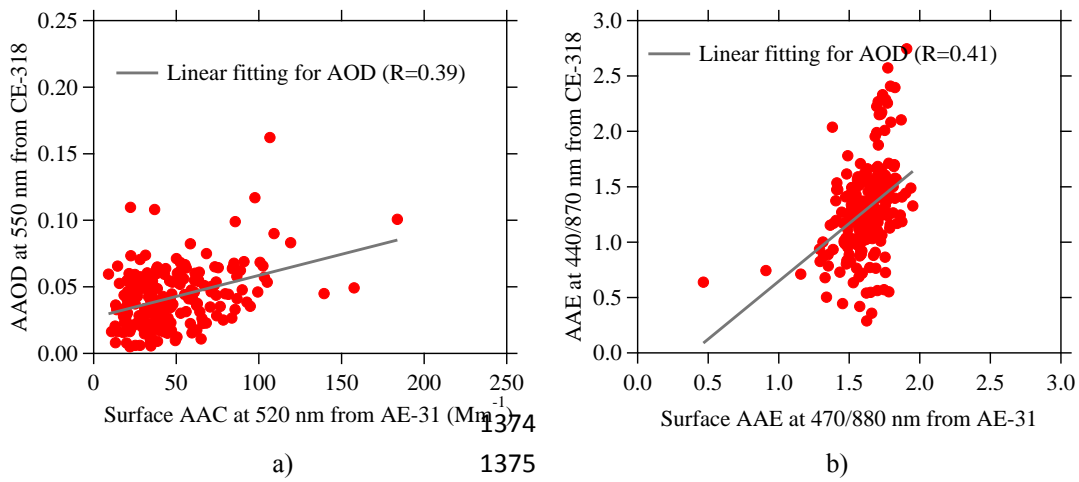
1367  
1368

Figure 6



1369  
1370  
1371

Figure 75

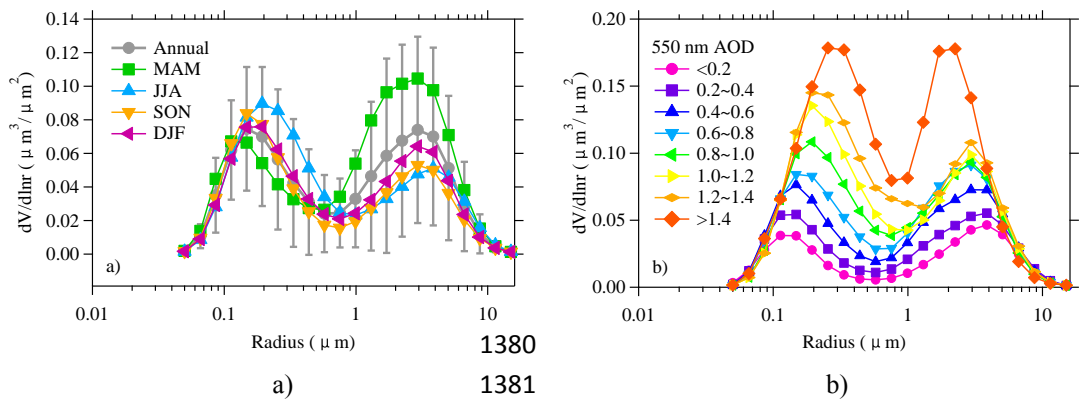


1372  
1373  
1376  
1377

1374

1375

Figure 86



1378  
1379  
1382  
1383

1380

1381

Figure 97

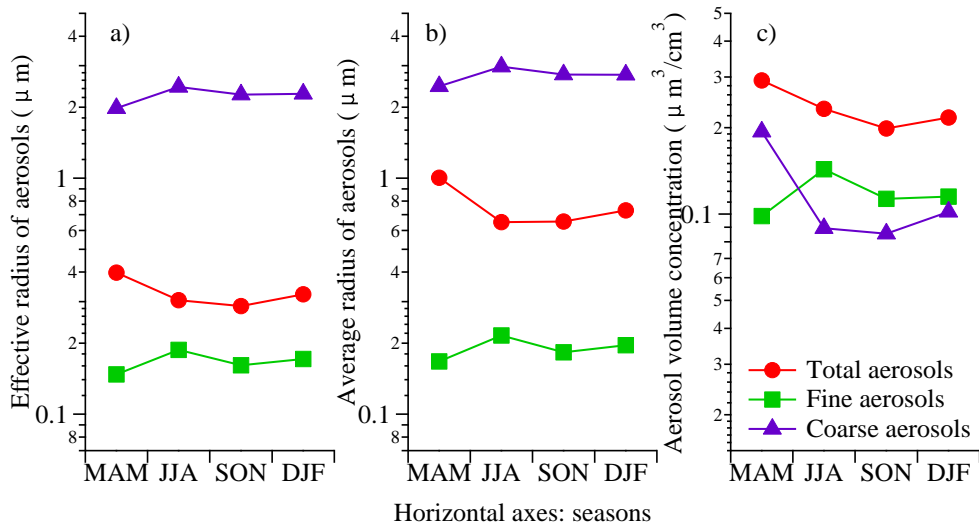


Figure 108

1384

1385

1386

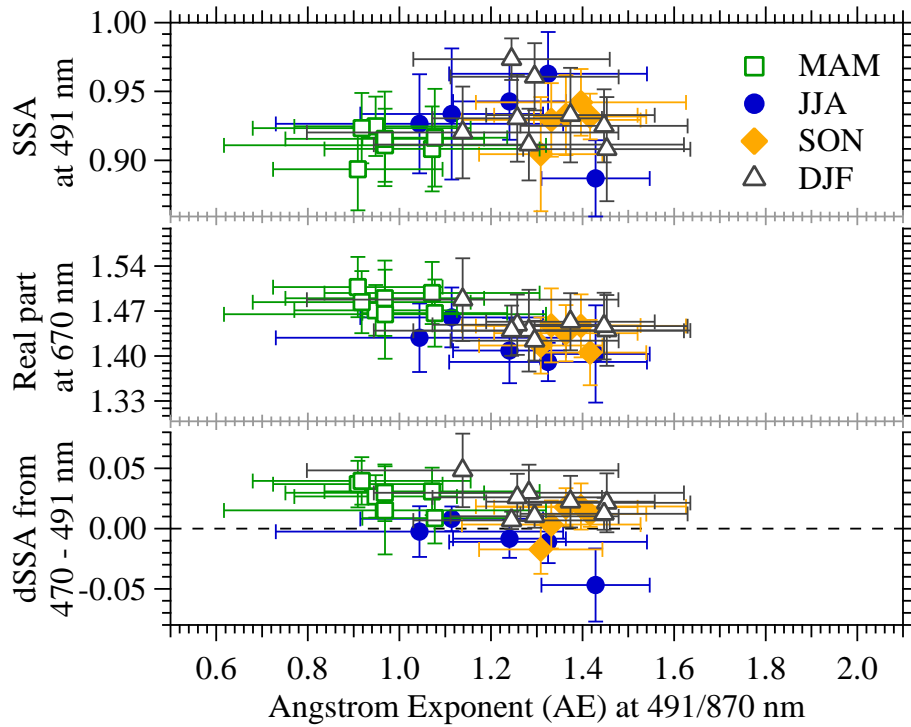


Figure 109

1387

1388

1389

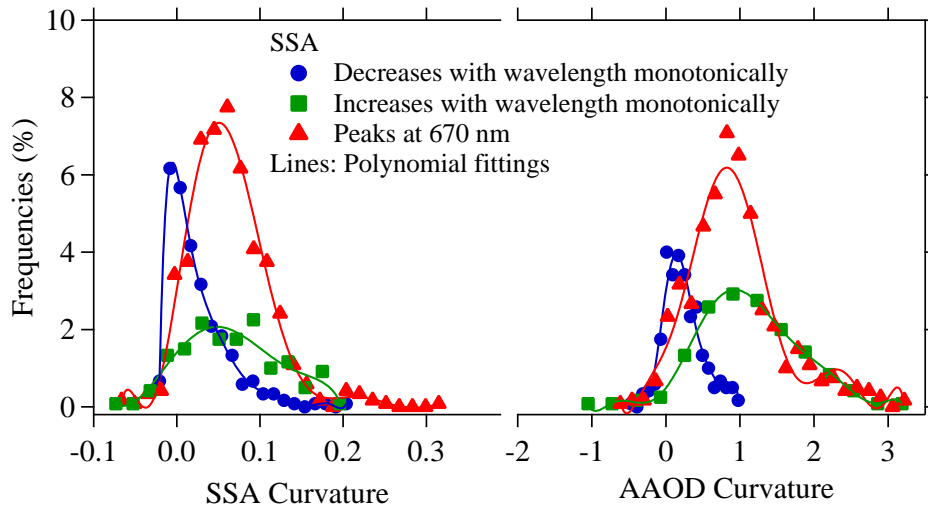


Figure 1210

1390  
1391  
1392

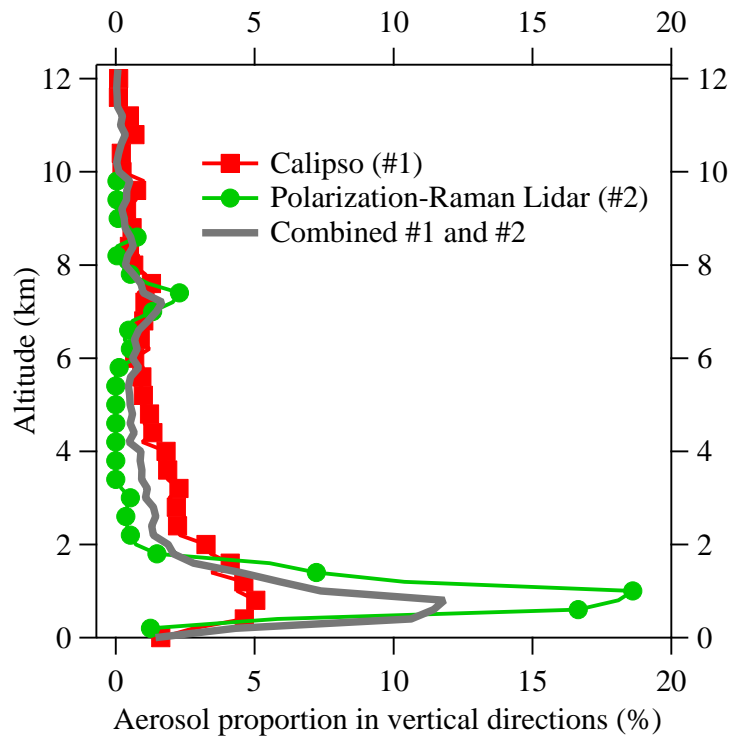
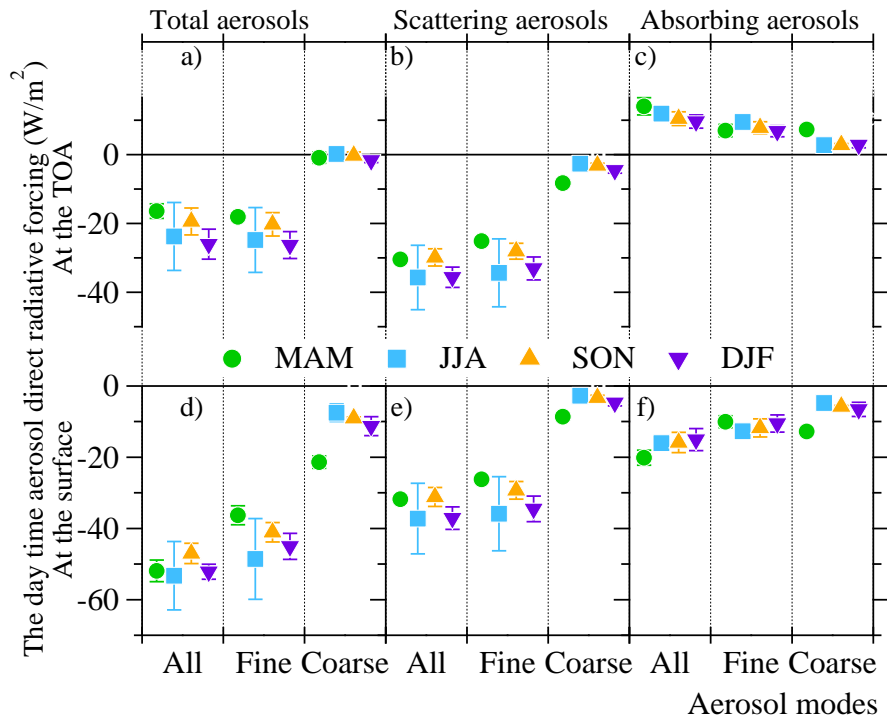


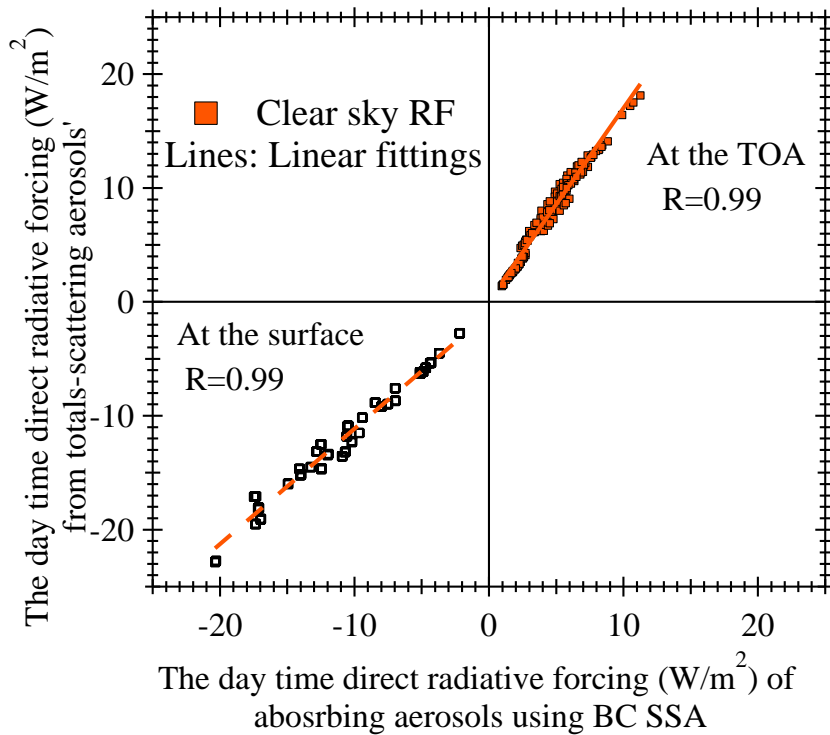
Figure 1311

1393  
1394  
1395



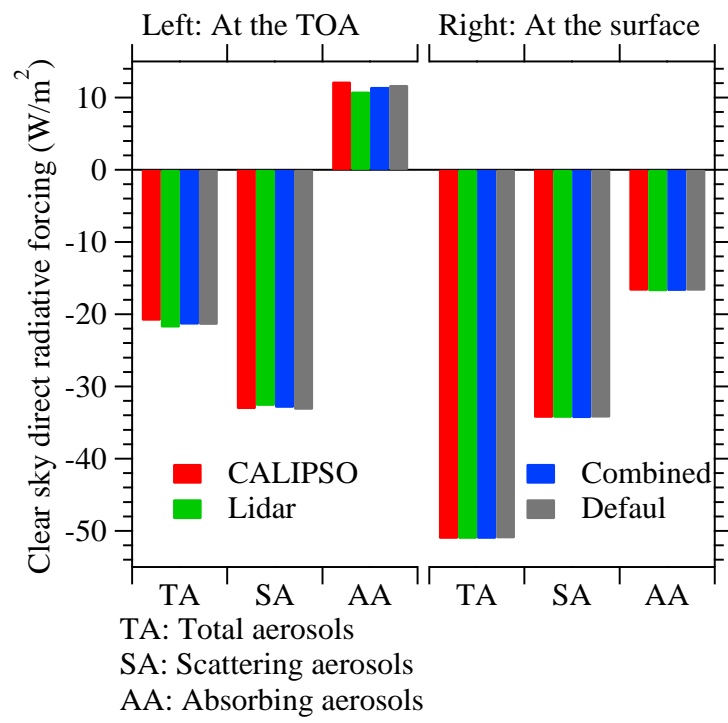
1396  
 1397  
 1398

Figure 1412



1399  
 1400  
 1401

Figure 1413



1402

1403

1404

1405

Figure 1614